REPORT DOCUMENTATION PAGE

Form Approved OMB NO. 0704-0188

1. REPORT DATE (DD-MM-YYYY)	2. REPORT TYPE	3. DATES COVERED (From - To)
15-12-2022	Final Report	16-Aug-2018 - 15-Sep-2022

4. TITLE AND SUBTITLE
Final Report: Understanding the instability of particle-laden liquids over soft porous media

5a. CONTRACT NUMBER
W911NF-18-1-0356

5b. GRANT NUMBER

5c. PROGRAM ELEMENT NUMBER
611102

6. AUTHORS

5d. PROJECT NUMBER

5e. TASK NUMBER

5f. WORK UNIT NUMBER

7. PERFORMING ORGANIZATION NAMES AND ADDRESSES
University of Illinois - Chicago
809 South Marshfield Avenue
MB 502, M/C 551
Chicago, IL 60612 -4305

8. PERFORMING ORGANIZATION REPORT NUMBER

9. SPONSORING/MONITORING AGENCY NAME(S) AND ADDRESS (ES)
U.S. Army Research Office
P.O. Box 12211
Research Triangle Park, NC 27709-2211

10. SPONSOR/MONITOR'S ACRONYM(S)
ARO

11. SPONSOR/MONITOR'S REPORT NUMBER(S)
73633-WS.42

12. DISTRIBUTION AVAILIBILITY STATEMENT
Approved for public release; distribution is unlimited.

13. SUPPLEMENTARY NOTES
The views, opinions and/or findings contained in this report are those of the author(s) and should not contrued as an official Department of the Army position, policy or decision, unless so designated by other documentation.

14. ABSTRACT

15. SUBJECT TERMS

16. SECURITY CLASSIFICATION OF:			17. LIMITATION OF ABSTRACT	15. NUMBER OF PAGES	19a. NAME OF RESPONSIBLE PERSON
a. REPORT	b. ABSTRACT	c. THIS PAGE			Parisa Mirbod
UU	UU	UU	UU		19b. TELEPHONE NUMBER 312-996-7389

RPPR Final Report
as of 19-Dec-2022

Agency Code: 21XD

Proposal Number: 73633WS **Agreement Number: W911NF-18-1-0356**
INVESTIGATOR(S):

Name: Ph.D. Parisa Mirbod Ph.D
Email: pmirbod@uic.edu
Phone Number: 3129967389
Principal: Y

Organization: **University of Illinois - Chicago**
Address: 809 South Marshfield Avenue, Chicago, IL 606124305
Country: USA
DUNS Number: 098987217 EIN: 376000511
Report Date: 15-Dec-2022 Date Received: 15-Dec-2022
Final Report for Period Beginning 16-Aug-2018 and Ending 15-Sep-2022
Title: Understanding the instability of particle-laden liquids over soft porous media
Begin Performance Period: 16-Aug-2018 **End Performance Period:** 15-Sep-2022
Report Term: 0-Other
Submitted By: Ph.D. Parisa Mirbod Email: pmirbod@uic.edu
Phone: (312) 996-7389
Distribution Statement: 1-Approved for public release; distribution is unlimited.

STEM Degrees: 3 **STEM Participants:** 6

Major Goals: The major goals of the proposed project are to quantitatively examine the suspension flows over porous media models (porous structures) and the related instabilities by developing and experimentally validating a new framework to model and understand the stability of the flow of particle-laden liquids in a rectangular channel in which one or two walls are coated with various porous media. The proposed concept, inspired by the nearly frictionless movement of red blood cells through tiny capillaries, involves covering the planar surfaces with specific porous material with permeability and porosity.

The specific objectives of the proposed project are aimed at achieving our major goal of developing and experimentally validating a new theoretical framework to model and understand this coupled flow and the causes of instability in the system.
In Objective# 1, the plan was to consider the pressure-driven channel flow of non-Brownian, non-colloidal particle-laden liquids at moderate to high concentrations (i.e., 0.05 to 0.5).
In Objective# 2, it was proposed to experimentally validate the theoretical predictions. We planned to design and construct an experimental test set-up and its supporting structures which will then allow us to flow suspensions in a channel over surfaces coated with and without a porous layer and to investigate the onset of instability. The set-up will be fully instrumented to measure the steady-state velocity and concentration profiles in the channel over the porous layer at low to moderate Reynolds numbers. We plan to perform the Osborne Reynolds experiment to define the onset of the instability in the system for dilute to concentrated suspensions. The slurry will be composed of poly(methylmethacrylate) (PMMA) particles with a mean radius of 100–150 microns. Particle concentrations of 1% to 50% will be tested. We employed particle image velocimetry (PIV) measurements to characterize the flow, and to define the velocity profiles, at dilute suspensions (1% and 5%). The magnetic resonance imaging (MRI) method was used to define the concentration distribution and velocity profiles for dilute to concentrated suspensions (1% and 50%). The data were compared with the analytical calculations performed in Objective 1. Discrepancies were noted, their potential sources have been investigated, and approaches to decreasing the errors have been explored.

Accomplishments: Please see uploaded document

RPPR Final Report
as of 19-Dec-2022

Training Opportunities: Two PhD candidates, one postdoc, and one master's student who worked on this project, Zhenxing Wu, Eileen A. Haffner, Indika Gayani Udagedara, and Saman Hooshyar, respectively, received both informal and formal technical training. Supported by a supplemental grant via the Army Educational Office Program (AEOP) in Summer 2019 allowed one undergraduate student (Eric Uribe) and one high school student (Namarata Acharya) to train and perform experiments using PIV in the PI's Lab and participate in group meetings and weekly presentations related to research methods.
As part of the informal training, the PI and her collaborators discussed theoretical and experimental methods and techniques of fluid dynamics, numerical methods, and dynamical systems on a regular basis. Participants and posdocs gave regular presentations at weekly group meetings, which included the PI and her collaborators, and several undergraduate and graduate students involved in particle-laden flows research. Among their professional development activities were relevant classwork, individual study of research-related topics, and active participation in the preparation of scientific papers and reports to the sponsor, as well as preparing and presenting talks about the research project. All graduate students presented their work at multiple annual meetings of the American Physical Society/Division of Fluid Dynamics. In Spring 2018, Zhenxing Wu defended his PhD thesis, and he is currently a postdoctoral fellow at Ohio State University, where he works on experimental and numerical fluid dynamics. In May 2021, Eileen A. Haffner was awarded a PhD, then she accepted a postdoctoral position at the University College London, UK to continue her work on the PIV/PTV. Due to a personal matter, Saman Hooshyar will have to get a MS degree instead of a PhD in May 2022.

Results Dissemination: The results of this research were disseminated through presentations at conferences, colloquia and seminars. In addition to the presentations at the ARO Program Review in 2016-2019, the PI (Parisa Mirbod) gave invited talks at the Argonne National Lab, Chicago (December 2022), University of Toledo, Department of Mechanical and Industrial Engineering (October 2022), University of Illinois, Urbana-Champaign, Department of Mechanical Engineering (May 2022), Okinawa Institute of Science and Technology Graduate University, Japan, Virtual (July 2021), Pual Shrerre Institute (PSI), Villigen, Switzerland (September 2019), the 10th InterPore Annual Meeting and Jubilee, invited Speaker, New Orleans (May 2018), Department of Biomedical Engineering, University of Wisconsin, Milwaukee, WI (April 2018), Department of Mechanical Engineering, San Diego State University, San Diego, California (Feb. 2018), and Department of Mechanical Engineering, City University of New York, New York, New York (Feb. 2018).

Graduate students and postdocs presented fourteen talks at various American Physical Society Division of Fluid Dynamics annual meetings. High-school classroom instruction via Zoom was carried out where the PI and her graduate researcher in Spring 2021 performed two virtual Zoom meetings at the Chicago, IL Central School to present two 30 minutes presentations regarding the bio-inspired strategies and how they can be applied in the science and engineering applications. This presentation reached approximately 40 high school choral members that were predominantly female.

This ARO award resulted in the publication of 12 papers. A paper in the Journal of Fluid Mechanics and another in the Journal of Rheology are in press. Currently, there are two papers in review: one was invited for a theme issue celebrating GI Taylor's 1923 in the Philosophical Transactions A, and the other is being reviewed in the Journal of Transport Phenomena.

Honors and Awards: 1) Editorial Member of the Scientific Journal (Nature Journal community), 2018- present.

2) President, External Affairs, APS Division of Fluid Dynamics (APS/DFD), 2021-2023.

3) Committee Member, InterPore Meeting, 2018-present.

Protocol Activity Status:

Technology Transfer: We have developed a new experimental method to be examined using PIV/PTV and Shake-the-Box in the PI's lab and also MRI in the Rutgers University. We
are currently working to file a patent for this specific experiment at UIC. An inventory has been reported as part of this project.

PARTICIPANTS:

Participant Type: PD/PI

Participant: Parisa Mirbod
Person Months Worked: 6.00 **Funding Support:**
Project Contribution:
National Academy Member: N

Participant Type: Co-Investigator
Participant: Nina Shapley
Person Months Worked: 3.00 **Funding Support:**
Project Contribution:
National Academy Member: N

Participant Type: Co-Investigator
Participant: Jonathan Higham
Person Months Worked: 3.00 **Funding Support:**
Project Contribution:
National Academy Member: N

Participant Type: Co-Investigator
Participant: Harunori Yoshikawa
Person Months Worked: 6.00 **Funding Support:**
Project Contribution:
National Academy Member: N

Participant Type: Co-Investigator
Participant: Luca Brandt
Person Months Worked: 3.00 **Funding Support:**
Project Contribution:
National Academy Member: N

Participant Type: Postdoctoral (scholar, fellow or other postdoctoral position)
Participant: Indika Gayani Udagedara
Person Months Worked: 6.00 **Funding Support:**
Project Contribution:
National Academy Member: N

Participant Type: Postdoctoral (scholar, fellow or other postdoctoral position)
Participant: Changwoo Kang
Person Months Worked: 8.00 **Funding Support:**
Project Contribution:
National Academy Member: N

Participant Type: Graduate Student (research assistant)
Participant: Zhenxing Wu
Person Months Worked: 12.00 **Funding Support:**

Project Contribution:
National Academy Member: N

Participant Type: Graduate Student (research assistant)
Participant: Eileen Haffner
Person Months Worked: 10.00 **Funding Support:**
Project Contribution:
National Academy Member: N

Participant Type: Graduate Student (research assistant)
Participant: Saman Hooshyar
Person Months Worked: 12.00 **Funding Support:**
Project Contribution:
National Academy Member: N

Participant Type: Undergraduate Student
Participant: Eric Uribe
Person Months Worked: 3.00 **Funding Support:**
Project Contribution:
National Academy Member: N

Participant Type: High School Student
Participant: Namrata Acharya
Person Months Worked: 3.00 **Funding Support:**
Project Contribution:
National Academy Member: N

Participant Type: Undergraduate Student
Participant: Joshua Ting
Person Months Worked: 3.00 **Funding Support:**
Project Contribution:
National Academy Member: N

Participant Type: Undergraduate Student
Participant: Kevin Lui
Person Months Worked: 3.00 **Funding Support:**
Project Contribution:
National Academy Member: N

RPPR Final Report
as of 19-Dec-2022

International Collaboration:

GBR

FRA

SWE

ARTICLES:

Publication Type: Journal Article Peer Reviewed: Y **Publication Status:** 1-Published
Journal: Physics of Fluids
Publication Identifier Type: DOI Publication Identifier: 10.1063/1.5021903
Volume: 30 Issue: 4 First Page #: 047103
Date Submitted: 11/29/18 12:00AM Date Published: 4/1/18 12:00AM
Publication Location:
Article Title: Experimental analysis of the flow near the boundary of random porous media
Authors: Zhenxing Wu, Parisa Mirbod
Keywords: PIV measurements, porous media, flow near the boundary
Abstract: The aim of this work is to experimentally examine flow over and near random porous media. Different porous materials were chosen to achieve porosity ranging from 0.95 to 0.99. In this study, we report the detailed velocity measurements of the flow over and near random porous material inside a rectangular duct using a planar particle image velocimetry (PIV) technique. By controlling the flow rate, two different Reynolds numbers were achieved. We determined the slip velocity at the interface between the porous media and free flow. Values of the slip velocity normalized either by the maximum flow velocity or by the shear rate at the interface and the screening distance K1/2 were found to depend on porosity. It was also shown that the depth of penetration inside the porous material was larger than the screening length using Brinkman's prediction. Moreover, we examined a model for the laminar coupled flow over and inside porous media and analyzed the permeability of a random porous medium.
Distribution Statement: 3-Distribution authorized to U.S. Government Agencies and their contractors
Acknowledged Federal Support: **Y**

Publication Type: Journal Article Peer Reviewed: Y **Publication Status:** 1-Published
Journal: Advances in Water Resources
Publication Identifier Type: Other Publication Identifier:
Volume: Issue: First Page #:
Date Submitted: 8/28/19 12:00AM Date Published: 6/15/19 5:00AM
Publication Location:
Article Title: Instability analysis of the flow between two parallel plates where the bottom one coated with porous media
Authors: Zhenxing Wu, Parisa Mirbod
Keywords: Coupled fluid-porous flow instability, Brinkman equation, Stability margin
Abstract: This study investigates the instability of pure Newtonian fluid flow between two parallel plates where the bottom one coated with various porous media with permeability K and porosity ?. We have applied normal modes to perturb the coupled flow system. Specifically, the effects of some dimensionless parameters such as depth ratio, permeability parameter, and the porosity of the porous medium on the instability have been examined. We found these parameters play a critical role in the instability. Depending on these parameters, instability is initiated and dominated either by the fluid or by the porous region. In particular, we found that there are ranges of the depth ratio and the permeability parameter for each value of the porous media porosity that affect the instability of this coupled flow. We have also determined a new parameter which specifies the potential dominance and the stability margin of each mode.
Distribution Statement: 3-Distribution authorized to U.S. Government Agencies and their contractors
Acknowledged Federal Support: **Y**

RPPR Final Report
as of 19-Dec-2022

Publication Type: Journal Article Peer Reviewed: Y **Publication Status:** 1-Published
Journal: Physical Review E
Publication Identifier Type: DOI Publication Identifier: 10.1103/PhysRevE.100.013109
Volume: 100 Issue: First Page #:
Date Submitted: 8/28/19 12:00AM Date Published: 7/22/19 3:00PM
Publication Location:
Article Title: Porosity effects in laminar fluid flow near permeable surfaces
Authors: Changwoo Kang, Parisa Mirbod
Keywords: laminar flow, porosity effects, scaling laws, kinetic energy
Abstract: This work analyzes the porosity effects on laminar flow and drag reduction of Newtonian fluids flowing over and through permeable surfaces. A fully developed laminar flow in a channel partially replaced with a porous material is considered. The analytical solutions for the velocity and shear stress are given and examined to identify the influence of the porosity on the flow. The scaling laws in the porous media are determined using asymptotic analysis in the limit of infinitely small permeability. Direct numerical simulations are performed and the transport equation for the kinetic energy is examined to establish the dependency of the porosity on the flow. We found that the impact of the porosity depends on the permeability. For high permeability, the higher porosity induces the increase of driving force and accelerates the flow while it decelerates the flow for low permeability by causing stronger viscous drag of the porous medium.
Distribution Statement: 3-Distribution authorized to U.S. Government Agencies and their contractors
Acknowledged Federal Support: **Y**

Publication Type: Journal Article Peer Reviewed: Y **Publication Status:** 1-Published
Journal: Rheologica Acta
Publication Identifier Type: DOI Publication Identifier:
Volume: 11 Issue: 60 First Page #:
Date Submitted: 12/14/22 12:00AM Date Published: 8/4/21 10:00AM
Publication Location:
Article Title: Pressure-driven pipe flow of semi-dilute and dense suspensions over permeable surfaces
Authors: Changwoo Kang and Parisa Mirbod
Keywords: particle-laden flows, pipe, drag reduction, porous media
Abstract: We study pressure-driven suspensions of non-colloidal and non-Brownian spheres in a Newtonian solvent where the pipe surface is replaced by porous media using direct numerical simulations. We examine various values of the permeability of the porous medium K, to clarify the effect of the permeable wall on the suspension flows at bulk particle volume fractions of 0.1 ? ?b ? 0.5. We find that in the limit of vanishing inertia, the rate of suspension flow decreases as the bulk volume fraction ?b increases and it builds up as the permeability of the porous media increases. We also show that there are two different regimes characterizing the slip velocity normalized by both shear rate and penetration depth, at the suspension-porous interface, namely the strong permeability regime and the weak permeability regime. In the former, the solvent penetrates deeper and the slip velocity increases with the permeability of porous media, while in the latter the variation of slip velocity is trivial.
Distribution Statement: 2-Distribution Limited to U.S. Government agencies only; report contains proprietary info
Acknowledged Federal Support: **Y**

RPPR Final Report
as of 19-Dec-2022

Publication Type: Journal Article Peer Reviewed: Y **Publication Status:** 1-Published
Journal: International Journal of Multiphase Flow
Publication Identifier Type: DOI Publication Identifier: doi.org/10.1016/j.ijmultiphaseflow.2020.1032
Volume: 126 Issue: First Page #:
Date Submitted: 8/30/20 12:00AM Date Published:
Publication Location:
Article Title: Shear-induced particle migration of semi-dilute and concentrated Brownian suspensions in both Poiseuille and circular Couette flow
Authors: Changwoo Kang, Parisa Mirbod
Keywords: Colloidal and Brownian suspensions, Shear-thinning effects, Particle migration, Poiseuille flow, Circular Couette flow
Abstract: This study explores thermal convection in suspensions of neutrally-buoyant, non-colloidal suspensions confined between horizontal walls. A constitutive diffusion equation is used to model the dynamics of the particles suspended in a viscous fluid and it is coupled with the flow equations. We employ a simple model that was proposed by Metzger, Rahli, and Yin (J. Fluid Mech. 724, 2013) for the effective thermal diffusivity of suspensions. This model considers the effects of shear-induced diffusion and gives the thermal diffusivity increasing linearly with the thermal Péclet number (Pe) and the particle volume fraction (?). Both linear stability analysis (LSA) and direct numerical simulation (DNS) are performed for various bulk particle volume fractions (?b) ranging from 0 to 0.3. Rac grows gradually by increasing ?b from the critical value (Rac=1708) for a pure fluid, while the critical wavenumber (kc) remains constant at 3.12.
Distribution Statement: 2-Distribution Limited to U.S. Government agencies only; report contains proprietary info
Acknowledged Federal Support: **Y**

Publication Type: Journal Article Peer Reviewed: Y **Publication Status:** 1-Published
Journal: Chemical Engineering Science
Publication Identifier Type: DOI Publication Identifier: 2020.116178
Volume: 230 Issue: First Page #:
Date Submitted: 12/14/22 12:00AM Date Published: 9/28/20 10:00AM
Publication Location:
Article Title: The impact of porous walls on the rheology of suspensions
Authors: Marco E. Rosti, Parisa Mirbod and Luca Brandt
Keywords: suspension rheology, porous media, fully resolved computations
Abstract: This study explores thermal convection in suspensions of neutrally-buoyant, non-colloidal suspensions confined between horizontal walls. A constitutive diffusion equation is used to model the dynamics of the particles suspended in a viscous fluid and it is coupled with the flow equations. We employ a simple model that was proposed by Metzger, Rahli, and Yin (J. Fluid Mech. 724, 2013) for the effective thermal diffusivity of suspensions. This model considers the effects of shear-induced diffusion and gives the thermal diffusivity increasing linearly with the thermal Péclet number (Pe) and the particle volume fraction (?). Both linear stability analysis (LSA) and direct numerical simulation (DNS) are performed for various bulk particle volume fractions (?b) ranging from 0 to 0.3. Rac grows gradually by increasing ?b from the critical value (Rac=1708) for a pure fluid, while the critical wavenumber (kc) remains constant at 3.12.
Distribution Statement: 2-Distribution Limited to U.S. Government agencies only; report contains proprietary info
Acknowledged Federal Support: **Y**

RPPR Final Report
as of 19-Dec-2022

Publication Type: Journal Article Peer Reviewed: Y **Publication Status:** 1-Published
Journal: Fluid Mechanics
Publication Identifier Type: DOI Publication Identifier: 2021.59
Volume: 915 Issue: A128 First Page #:
Date Submitted: 8/27/21 12:00AM Date Published:
Publication Location:
Article Title: Onset of thermal convection in non-colloidal suspensions
Authors: Changwoo Kang, Harunori N. Yoshikawa, and Parisa Mirbod
Keywords: Non-colloidal, Non-Brownian, Concentrated suspensions, Rayleigh-Bénard convection, Shear-induced diffusion
Abstract: This study explores thermal convection in suspensions of neutrally-buoyant, non-colloidal suspensions confined between horizontal walls. A constitutive diffusion equation is used to model the dynamics of the particles suspended in a viscous fluid and it is coupled with the flow equations. We employ a simple model that was proposed by Metzger, Rahli, and Yin (J. Fluid Mech. 724, 2013) for the effective thermal diffusivity of suspensions. This model considers the effects of shear-induced diffusion and gives the thermal diffusivity increasing linearly with the thermal Péclet number (Pe) and the particle volume fraction (?). Both linear stability analysis (LSA) and direct numerical simulation (DNS) are performed for various bulk particle volume fractions (?b) ranging from 0 to 0.3. Rac grows gradually by increasing ?b from the critical value (Rac=1708) for a pure fluid, while the critical wavenumber (kc) remains constant at 3.12.
Distribution Statement: 2-Distribution Limited to U.S. Government agencies only; report contains proprietary info
Acknowledged Federal Support: **Y**

Publication Type: Journal Article Peer Reviewed: Y **Publication Status:** 1-Published
Journal: Fluid Mechanics
Publication Identifier Type: DOI Publication Identifier: 2021.75
Volume: 916 Issue: First Page #:
Date Submitted: 8/27/21 12:00AM Date Published: 1/17/21 6:00AM
Publication Location:
Article Title: Flow instability and transitions in Taylor–Couette flow of a semidilute non-colloidal suspension
Authors: Changwoo Kang, Parisa Mirbod
Keywords: instability control, suspensions, Taylor–Couette flow
Abstract: Flow of a semidilute neutrally buoyant and non-colloidal suspension is numerically studied in the Taylor–Couette geometry where the inner cylinder is rotating and the outer one is stationary. We consider a suspension with bulk particle volume fraction ?b = 0.1, the radius ratio (? = ri/ro = 0.877) and two particle size ratios ? (= d/a) = 60, 200, where d is the gap width (= ro ? ri) between cylinders, a is the suspended particles' radius and ri and ro are the inner and outer radii of the cylinder, respectively. Numerical simulations are conducted using the suspension balance model (SBM) and rheological constitutive laws. We predict the critical Reynolds number in which counter-rotating vortices arise in the annulus. It turns out that the primary instability appears through a supercritical bifurcation. For the suspension of ? = 200, the circular Couette flow (CCF) transitions via Taylor vortex flow (TVF) to wavy vortex flow (WVF).
Distribution Statement: 2-Distribution Limited to U.S. Government agencies only; report contains proprietary info
Acknowledged Federal Support: **Y**

RPPR Final Report
as of 19-Dec-2022

Publication Type: Journal Article Peer Reviewed: Y **Publication Status:** 1-Published
Journal: Engineering Mathematics
Publication Identifier Type: Other Publication Identifier:
Volume: 132 Issue: 1 First Page #: 1
Date Submitted: 12/14/22 12:00AM Date Published:
Publication Location:
Article Title: The impact of imposed Couette on the stability of pressure- driven flows over porous surfaces
Authors: Saman Hooshyar, Harunori N. Yoshikawa and Parisa Mirbod
Keywords: Linear instability, Plane Poiseuille-Couette flow, Porous media surface, Darcy- Brinkman equation
Abstract: We present linear stability analysis of a pressure-driven flow in a fluid-layer overlaying porous media due to the imposed Couette component. We model the flow dynamics in the porous media by the Brinkman equation, considering small permeability, and couple it with the Navier-Stokes equation for flows in the fluid-layer. The effect of the upper impermeable wall velocity, which generates the Couette flow component, on flow stability is discussed in detail with varying the permeability and thickness of the fluid layer. The results show that a Couette flow component at first exerts destabilizing effects on the system but as the wall velocity gradually increases, the flow component eventually stabilizes. The cutoff velocity, at which the critical Reynolds number of Poiseuille-Couette flow (PCF) is the same as the critical Reynolds number corresponding to Poiseuille flow (PF), is highly dependent on the porous medium characteristics.
Distribution Statement: 3-Distribution authorized to U.S. Government Agencies and their contractors
Acknowledged Federal Support: **Y**

Publication Type: Journal Article Peer Reviewed: Y **Publication Status:** 1-Published
Journal: Physics of Fluids
Publication Identifier Type: Publication Identifier:
Volume: 32 Issue: 083608 First Page #:
Date Submitted: 12/14/22 12:00AM Date Published: 1/15/20 3:10AM
Publication Location:
Article Title: Velocity measurements of a dilute particulate suspension over and through a porous medium model
Authors: Eileen A. Haffner, Parisa Mirbod
Keywords: Particle Image velocimetry, dilute suspensions, low Reynolds regime
Abstract: We experimentally examine pressure-driven flows of 1%, 3%, and 5% dilute suspensions over and through a porous media model. The flow of non-colloidal, non-Brownian suspensions of rigid and spherical particles suspended in a Newtonian fluid is considered at very low Reynolds numbers. The model of porous media consists of square arrays of rods oriented across the flow in a rectangular channel. Systematic experiments using high-spatial-resolution planar particle image velocimetry (PIV) and index-matching techniques are conducted to accurately measure the velocity measurements of both very dilute and solvent flows inside and on top of the porous media model. We found that for 1%, 3%, and 5% dilute suspensions the fully-developed velocity profile inside the free-flow region are well predicted by the exact solution derived from coupling the Navier-Stokes equation within the free flow-region and the volume-averaged Navier Stokes (VANS) equation for the porous media.
Distribution Statement: 2-Distribution Limited to U.S. Government agencies only; report contains proprietary info
Acknowledged Federal Support: **Y**

RPPR Final Report
as of 19-Dec-2022

Publication Type: Journal Article Peer Reviewed: Y **Publication Status:** 1-Published
Journal: Journal of Fluid Mechanics
Publication Identifier Type: DOI Publication Identifier:
Volume: 945 Issue: A6 First Page #:
Date Submitted: 12/14/22 12:00AM Date Published: 8/22/22 5:00AM
Publication Location:
Article Title: Turbulent Rayleigh–Bénard convection in non-colloidal suspensions
Authors: Andreas D Demou, Mehdi Niazi Ardekani, Parisa Mirbod, Luca Brandt
Keywords: Turbulent flow, suspensions, Rayleigh-Benard convection
Abstract: This study presents direct numerical simulations of turbulent Rayleigh–Bénard convection in non-colloidal suspensions, with special focus on the heat transfer modifications in the flow. Adopting a Rayleigh number of and 40 % are observed in all statistical quantities, including heat transfer and turbulent kinetic energy budgets, and two-point correlations. Special attention is also given to the role of particle rotation, which is shown to contribute to maintaining high heat transfer rates in moderate volume fractions. Furthermore, decreasing the particle size promotes the particle layering next to the wall, inducing a similar heat transfer reduction as in the highest particle volume fraction case.
Distribution Statement: 1-Approved for public release; distribution is unlimited.
Acknowledged Federal Support: **Y**

Publication Type: Journal Article Peer Reviewed: Y **Publication Status:** 2-Awaiting Publicat
Journal: Journal of Fluid Mechanics
Publication Identifier Type: Publication Identifier:
Volume: Issue: First Page #:
Date Submitted: 12/14/22 12:00AM Date Published: 12/19/22 12:00PM
Publication Location:
Article Title: Turbulent channel flow of suspensions of neutrally buoyant particles over porous media
Authors: Parisa Mirbod. Seyedmehdi Abtahi, Abbas Moradi Bilondi, Marco Edoardo Rosti, Luca Brandt
Keywords: Turbulent flow, suspensions, porous media
Abstract: This study discusses turbulent suspension flows of non-Brownian, non-colloidal, neutrally buoyant and rigid spherical particles in a Newtonian fluid over porous media with particles too large to penetrate and move through the porous layer. We consider suspension flows with the solid volume fraction ranging from 0 to 0.2, and different wall permeabilities, while porosity is constant at 0.6. Direct numerical simulations with an immersed boundary method are employed to resolve the particles and flow phase, with the volume-averaged Navier–Stokes equations modelling the flow within the porous layer. The results show that in the presence of particles in the free-flow region, the mean velocity and the concentration profiles are altered with increasing porous layer permeability because of the variations in the slip velocity and wall-normal fluctuations at the suspension-porous interface.
Distribution Statement: 3-Distribution authorized to U.S. Government Agencies and their contractors
Acknowledged Federal Support: **Y**

RPPR Final Report
as of 19-Dec-2022

Publication Type: Journal Article Peer Reviewed: Y **Publication Status:** 2-Awaiting Publicat
Journal: Philosophical Transactions A theme issue: celebrating the centennial of GI Taylor's 1923 paper
Publication Identifier Type: Publication Identifier:
Volume: Issue: First Page #:
Date Submitted: 12/14/22 12:00AM Date Published: 1/9/23 6:00AM
Publication Location:
Article Title: Transitions in Taylor-Couette flow of concentrated non-colloidal suspensions
Authors: Changwoo Kang, Parisa Mirbod
Keywords: Non-colloidal, Non-Brownian, Concentrated suspension, Taylor-Couette flow
Abstract: Taylor-Couette flow of concentrated non-colloidal suspensions with the rotating inner cylinder and the stationary outer one is numerically investigated. We consider suspensions of the bulk particle volume fraction 0.2, 0.3 with the ratio of annular gap to the particle radius "? = 60" confined in a cylindrical annulus of the radius ratio (i.e., ratio of inner and outer diameters) "? = 0.877" . Numerical simulations are performed by applying suspension-balance model and rheological constitutive laws. To observe flow patterns caused by suspended particles, the Reynolds number of the suspension, based on the bulk particle volume fraction and the rotating velocity of the inner cylinder, is varied up to 180. At high Reynold number, modulated patterns undiscovered in the flow of a semi-dilute suspension emerge beyond a wavy vortex flow.
Distribution Statement: 2-Distribution Limited to U.S. Government agencies only; report contains proprietary info
Acknowledged Federal Support: **Y**

Publication Type: Journal Article Peer Reviewed: Y **Publication Status:** 4-Under Review
Journal: Journal of Transport Phenomena
Publication Identifier Type: Publication Identifier:
Volume: Issue: First Page #:
Date Submitted: 12/14/22 12:00AM Date Published: 1/17/23 12:00PM
Publication Location:
Article Title: Linear stability analysis of particle-laden flows in channels with porous walls
Authors: Parisa Mirbod, Saman Hooshyar, Elmira Taheri, Harunori N. Yoshikawa
Keywords: Linear stability, Dusty gas model, Particle-laden flows, porous media
Abstract: Laboratory experiments were conducted to study particle migration and flow properties of non-Brownian, non-colloidal suspensions ranging from 10% to 40% particle volume fraction in a pressure-driven flow over and through a porous structure at low Reynolds number. Particle concentration maps, velocity maps and corresponding profiles were acquired using a magnetic resonance imaging (MRI) technique. The model porous medium consists of square arrays of circular rods oriented across the flow in a rectangular microchannel. It was observed that the square arrays of the circular rods modify the velocity profiles and result in heterogeneous concentration fields for various suspensions. As the bulk particle volume fraction of the suspension increases, particles tend to concentrate in the free channel relative to the porous medium while the centerline velocity profile along the lateral direction becomes increasingly blunted.
Distribution Statement: 2-Distribution Limited to U.S. Government agencies only; report contains proprietary info
Acknowledged Federal Support: **Y**

RPPR Final Report
as of 19-Dec-2022

Publication Type: Journal Article Peer Reviewed: Y **Publication Status:** 2-Awaiting Publicat
Journal: Journal of Rheology
Publication Identifier Type: Publication Identifier:
Volume: Issue: First Page #:
Date Submitted: 12/14/22 12:00AM Date Published: 12/2/22 6:00AM
Publication Location:
Article Title: Particle migration of suspensions in a pressure-driven flow over and through a porous structure
Authors: Parisa Mirbod, Nina C. Shapley
Keywords: Magnetic resonance imaging, suspensions, pressure driven flow, banding
Abstract: Laboratory experiments were conducted to study particle migration and flow properties of non-Brownian, non-colloidal suspensions ranging from 10% to 40% particle volume fraction in a pressure-driven flow over and through a porous structure at low Reynolds number. Particle concentration maps, velocity maps and corresponding profiles were acquired using a magnetic resonance imaging (MRI) technique. The model porous medium consists of square arrays of circular rods oriented across the flow in a rectangular microchannel. It was observed that the square arrays of the circular rods modify the velocity profiles and result in heterogeneous concentration fields for various suspensions. As the bulk particle volume fraction of the suspension increases, particles tend to concentrate in the free channel relative to the porous medium while the centerline velocity profile along the lateral direction becomes increasingly blunted.
Distribution Statement: 2-Distribution Limited to U.S. Government agencies only; report contains proprietary info
Acknowledged Federal Support: **Y**

CONFERENCE PAPERS:

Publication Type: Conference Paper or Presentation **Publication Status:** 1-Published
Conference Name: American Physical Society- Division of Fluid dynamics
Date Received: 29-Nov-2018 Conference Date: 18-Nov-2018 Date Published: 20-Nov-2018
Conference Location: Atlanta, GA
Paper Title: instability of the flow between two parallel palates where the bottom one coated with porous media
Authors: Zhenxing Wu, Parisa Mirbod
Acknowledged Federal Support: **Y**

Publication Type: Conference Paper or Presentation **Publication Status:** 1-Published
Conference Name: American Physical Society
Date Received: 29-Nov-2018 Conference Date: 18-Nov-2018 Date Published: 20-Nov-2018
Conference Location: Atlanta, GA
Paper Title: PIV measurements of dilute suspension flows over porous medium models
Authors: Eileen Haffner, Byron Erath, Parisa Mirbod
Acknowledged Federal Support: **Y**

Publication Type: Conference Paper or Presentation **Publication Status:** 1-Published
Conference Name: 10th InterPore Annual Meeting and Jubilee
Date Received: 29-Nov-2018 Conference Date: 14-May-2018 Date Published: 17-May-2018
Conference Location: New Orleans, Louisiana, USA
Paper Title: Flow and transport of particle-laden liquids over permeable surfaces; Theory and experiment
Authors: Parisa Mirbod
Acknowledged Federal Support: **Y**

RPPR Final Report
as of 19-Dec-2022

Publication Type: Conference Paper or Presentation **Publication Status:** 1-Published
Conference Name: American Physical Society-Division of Fluid Dynamics
Date Received: 29-Nov-2018 Conference Date: 05-Mar-2018 Date Published: 09-Mar-2018
Conference Location: Los Angeles, California, USA
Paper Title: Flow near the boundary of random soft porous media
Authors: Zhenxing Wu, Parisa Mirbod
Acknowledged Federal Support: **Y**

Publication Type: Conference Paper or Presentation **Publication Status:** 1-Published
Conference Name: American Physical Society-Division of Fluid Dynamics
Date Received: 28-Aug-2019 Conference Date: 08-Nov-2018 Date Published: 20-Nov-2018
Conference Location: Atlanta, Georgia
Paper Title: Instability analysis of the flow between two parallel plates where the bottom one coated with porous media
Authors: Zhenxing Wu and Parisa Mirbod
Acknowledged Federal Support: **Y**

Publication Type: Conference Paper or Presentation **Publication Status:** 1-Published
Conference Name: American Physical Society-DFD
Date Received: 29-Aug-2021 Conference Date: 22-Nov-2019 Date Published:
Conference Location: Seattle, WA
Paper Title: Particle migration of colloidal and Brownian suspen- sions in both Poiseuille and circular Couette flow
Authors: Changwoo Kang, Parisa Mirbod
Acknowledged Federal Support: **Y**

Publication Type: Conference Paper or Presentation **Publication Status:** 1-Published
Conference Name: American Physical Society-DFD
Date Received: 29-Aug-2021 Conference Date: 22-Nov-2019 Date Published:
Conference Location: Seattle, WA
Paper Title: Linear stability analysis of plane Poiseuille-Couette flow over a permeable surface
Authors: Saman Hooshyar, Parisa Mirbod
Acknowledged Federal Support: **Y**

Publication Type: Conference Paper or Presentation **Publication Status:** 1-Published
Conference Name: American Physical Society-DFD
Date Received: 29-Aug-2021 Conference Date: 22-Nov-2019 Date Published:
Conference Location: Seattle, WA
Paper Title: Instability analysis of Poiseuille flow between two par- allel walls partially obstructed by porous surfaces
Authors: Namrata Acharya, Saman Hooshyar, Parisa Mirbod
Acknowledged Federal Support: **Y**

Publication Type: Conference Paper or Presentation **Publication Status:** 1-Published
Conference Name: American Physical Society-DFD
Date Received: 29-Aug-2021 Conference Date: 22-Nov-2019 Date Published:
Conference Location: Seattle, WA
Paper Title: Experimental analysis of dilute particle-laden liquids over and through patterned structures
Authors: Eileen Haffner, Jonathan Higham, Parisa Mirbod
Acknowledged Federal Support: **Y**

RPPR Final Report
as of 19-Dec-2022

Publication Type: Conference Paper or Presentation **Publication Status:** 1-Published
Conference Name: American Physical Society-DFD
Date Received: 29-Aug-2021 Conference Date: 22-Nov-2019 Date Published:
Conference Location: Seattle, WA
Paper Title: Experimental and numerical studies of particle-laden fluid flows over a porous media model
Authors: Eileen Haffner, Changwoo Kang, Nina Shapely, Parisa Mirbod
Acknowledged Federal Support: **Y**

Publication Type: Conference Paper or Presentation **Publication Status:** 1-Published
Conference Name: The American Physical Society-DFD
Date Received: 29-Aug-2021 Conference Date: 23-Nov-2020 Date Published:
Conference Location: Chicago, IL (VIRTUAL)
Paper Title: Numerical study of a semi-dilute, non-colloidal sus- pension in a Taylor-Couette flow
Authors: Changwoo Kang, Parisa Mirbod
Acknowledged Federal Support: **Y**

Publication Type: Conference Paper or Presentation **Publication Status:** 1-Published
Conference Name: The American Physical Society-DFD
Date Received: 29-Aug-2021 Conference Date: 23-Nov-2020 Date Published:
Conference Location: Chicago, IL (VIRTUAL)
Paper Title: Rayleigh-Benard convection in non-colloidal suspensions
Authors: Changwoo Kang, Harunori Yoshikawa, Parisa Mirbod
Acknowledged Federal Support: **Y**

Publication Type: Conference Paper or Presentation **Publication Status:** 1-Published
Conference Name: The American Physical Society-DFD
Date Received: 29-Aug-2021 Conference Date: 24-Nov-2020 Date Published:
Conference Location: Chicago, IL (VIRTUAL)
Paper Title: Turbulent Channel Flow of Suspensions over Porous Media
Authors: Seyedmehdi Abtahi, Marco Rosti, Luca Brandt, Parisa Mirbod
Acknowledged Federal Support: **Y**

Publication Type: Conference Paper or Presentation **Publication Status:** 1-Published
Conference Name: The American Physical Society-DFD
Date Received: 29-Aug-2021 Conference Date: 24-Nov-2020 Date Published:
Conference Location: Chicago, IL (VIRTUAL)
Paper Title: Energy budget analysis of plane Poiseuille-Couette flow over a permeable surface
Authors: Saman Hooshyar, Harunori Yoshikawa, Parisa Mirbod
Acknowledged Federal Support: **Y**

Publication Type: Conference Paper or Presentation **Publication Status:** 1-Published
Conference Name: 25th International Congress of Theoretical and Applied Mechanics
Date Received: 29-Aug-2021 Conference Date: 25-Aug-2021 Date Published:
Conference Location: Milan, ITALY (VIRTUAL)
Paper Title: TRANSITIONS IN A TAYLOR-COUETTE FLOW OF DILUTE NON-COLLOIDAL SUSPENSIONS
Authors: Changwoo Kang, Parisa Mirbod
Acknowledged Federal Support: **Y**

RPPR Final Report
as of 19-Dec-2022

Publication Type: Conference Paper or Presentation **Publication Status:** 1-Published
Conference Name: American Physical Society-DFD
Date Received: 14-Dec-2022 Conference Date: 20-Nov-2022 Date Published:
Conference Location: Indianapolis, IN
Paper Title: Multi-phase Turbulent Rayleigh-Benard convection with bubbles
Authors: Abbas Moradi Bilondi, Nicolo Scapin, Luca Brandt, Parisa Mirbod
Acknowledged Federal Support: **Y**

Publication Type: Conference Paper or Presentation **Publication Status:** 1-Published
Conference Name: American Physical Society-DFD
Date Received: 14-Dec-2022 Conference Date: 21-Nov-2022 Date Published:
Conference Location: Indianapolis, IN
Paper Title: Turbulent flow of polymer solutions in a square duct roughened with transverse ribs
Authors: Abbas Moradi Bilondi, Nazario Mastroianni, Luca Brandt, Parisa Mirbod
Acknowledged Federal Support: **Y**

Publication Type: Conference Paper or Presentation **Publication Status:** 1-Published
Conference Name: American Physical Society-DFD
Date Received: 14-Dec-2022 Conference Date: 21-Nov-2022 Date Published:
Conference Location: Indianapolis, IN
Paper Title: The effect of viscoelastic flow on instabilities of plane Poiseuille problem with walls porous
Authors: Elmira Taheri, Harunori N. Yoshikawa, Parisa Mirbod
Acknowledged Federal Support: **Y**

Publication Type: Conference Paper or Presentation **Publication Status:** 1-Published
Conference Name: American Physical Society-DFD
Date Received: 14-Dec-2022 Conference Date: 21-Nov-2022 Date Published:
Conference Location: Indianapolis, IN
Paper Title: Linear Stability Analysis of a Particle laden Poiseuille Couette flow over a porous layer
Authors: Samir Popli, Parisa Mirbod, Harunori N. Yoshikawa
Acknowledged Federal Support: **Y**

DISSERTATIONS:

Publication Type: Thesis or Dissertation
Institution: University of Illinois at Chicago
Date Received: 27-Aug-2021 Completion Date: 3/13/21 3:00AM
Title: Experimental Analysis of Suspension Flows Over and Through Various Porous Media Models
Authors: Eileen A. Haffner
Acknowledged Federal Support: **Y**

RPPR Final Report
as of 19-Dec-2022

Partners

,

I certify that the information in the report is complete and accurate:
Signature: Parisa Mirbod
Signature Date: 12/15/22 3:57PM

1. Scientific Background and Motivation

1.1. Microcirculation and Glycocalyx

The possibility of using porous, highly compressible materials as lubricating layers is a new concept that has grown out of several fundamental biological questions related to the role of the fiber matrix layers that surround cells in an *in vivo* fluid environment [2]. For instance, in experimental studies of blood flow in microvessels, it was found that red blood cells experience much less friction than predicted by theory [4]. This was because of the presence of a relatively thick (~1 μm) layer of macromolecules bound to the endothelial cells lining the microvessel walls [5, 6], which affects interactions of blood cells with vessel walls [7]. This layer, which is located on the luminal surface of vascular cells, is called the endothelial glycocalyx layer (EGL) (Figure 1A). Computer-enhanced images showed that the glycocalyx is a 3D fibrous mesh network that forms a hexagonal array with an inter-cluster spacing (typically 100 nm in frog lung capillaries) [8]. The EGL also provides a red blood cell "exclusion zone" or "gap" between the flowing red blood cells and the endothelial membrane as shown in Figure 1B. A lubrication theory was developed by [9] for red cells and soft porous media and it was predicted that greatly enhanced lift forces could be produced in the glycocalyx layer at velocities >20 μm/s due to the large increase in pressure in the trapped porous layer between the red cell and the endothelial cell membrane. In [8], the authors proposed that the EGL's ability to restore itself is due to the flexural rigidity EI of the core proteins, the major structural component of the EGL, where E and I are the Young's modulus and moment of inertia of the core proteins, respectively. The PI extended the lubrication theory to randomly oriented porous media. It was shown that the excess pore pressure generated by a surface moving on any compressible porous media scales as permeability parameter $\alpha^2 = h^2/K$, for $\alpha >> 1$ where α is of order 10^2 or larger (h is the thickness and K is the permeability of the porous media) [10, 11]. While the PI's previous work [10, 11], focused on analytical modeling of the lubrication theory for the highly compressible porous media and its application in designing a new train track, the proposed project explores entirely different phenomena: porous media, with envisioned application to the flow of particle-laden flows as well as fundamental understanding of the instability in the system [12, 13]. In this project, we used porous structures with the similar properties as of EGL to mimic the EGL and to be able to understand the flow and instabilities in the system.

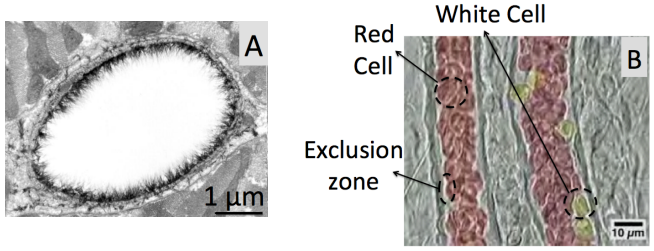

Figure 1. (A) Endothelial glycocalyx of a rat left ventricular myocardial capillary stained with Alcian blue 8GX and visualized using electron microscopy. (Adapted from [1]). **(B)** Motion of red and white blood cells in an arteriole [3].

1.2 Current understanding of the stability of suspensions and flow over porous media

Migration of non-Brownian particles of suspensions in smooth channels has been well studied both numerically [14, 15] and experimentally [16-18]. Particle migration has been much studied beginning the work presented by [19]. In these cases, despite the apparently stable low Reynolds flow, some transient sub-structural near-wall features in the concentration profiles such as ripples have been observed in experimental data. Inspired by this work, the instability of the pressure-driven, low Reynolds flow of Brownian suspensions with spherical particles in a microchannel has

been reported in detail by [20]. The authors were able to determine the unstable modes of Brownian suspensions in a microchannel using analytical methods.

The stability analysis of pure Newtonian fluids over porous layers has also received considerable attention. The flows in bounded domains such as Poiseuille flows over porous layers has been examined by [21, 22], flows of films on porous inclined planes by [23, 24], convection through porous layers by [22, 25, 26]. Instabilities were found in a single fluid-porous system. It was also found that the depth ratio, porosity, and the permeability parameters play a critical role in these instabilities. **However, to the PI's knowledge, stability analysis of suspensions in a channel coated with porous media has never before been addressed neither analytically nor experimentally.**

The two different models to describe the dynamics of suspension flow are: 1) The diffusive flux model (DFM), introduced by [19, 27], which is phenomenological and involves the diffusion fluxes of particles due to particle collisions with the spatial variation in the viscosity, and 2) The suspension balance model (SBM) that starts from the conservation equations of mass, momentum, and energy for the fluid and particle phases [14, 15] and takes into account normal stress differences to handle curvilinear flows.

Experimental findings show that small but finite inertia is the cause of interesting effects in a pressure driven pipe flow of suspensions [28-32]. The theoretical analysis on a single particle in Poiseuille flow reveals the existence of a lateral force acting on the particle [31-33]. An experimental study of inertial migration of dense suspensions using MRI provided insights into concentration profiles at varying bulk concentrations and particle Reynolds number [34]. Different fully developed concentration profiles for the different sized particles in pipe flow have been reported by [35]. In addition, flow-induced migration has been examined in [19, 36]. In this project, the constitutive model proposed by [14, 15] will be used to elucidate the dynamics of suspensions. Recently, the PI has also examined particle migration in an eccentric journal bearing using SBM [37]. Herein, the inertial effects will be taken into account by introducing the lift force term in the particle phase momentum balance and proposing a constitutive law relating the mixture stress to the local rate of strain with Reynolds number effects on the stress included by [38]. *Thus, in this project the suspension balance model will be coupled with the Brinkman equation to investigate the behavior of the interaction of the two regimes and to characterize the stability of the flow in the system.*

Experimental studies and direct analysis of the flow over and through porous media have been conducted using particle image velocimetry (PIV) [39-41] and laser Doppler anemometry (LDA) [42, 43]. The velocity profile of a fluid undergoing simple shear above a porous medium (commercial sandpapers with three different grits) was experimentally investigated. Optical measurement techniques are now routinely used in experimental fluid mechanics to investigate dilute and concentrated suspensions as well as pure Newtonian fluids. For instance, MRI [44-48], Laser-Doppler velocimetry (LDV) and PIV [49] are now increasingly used to visualize flow behavior. The main advantage of MRI over optical methods in examining concentrated suspensions is the ability to measure the concentration and velocity profiles in highly scattering or opaque systems [44]. The instability of the Poiseuille flow of pure fluid using experiments has been studied in[50] and references therein].

To sum up, the objective of the proposed project is to quantitatively investigate the suspension flows over porous media and the related instabilities by developing and experimentally validating a new framework to model and to understand the stability of the flow of particle-laden liquids in a rectangular channel in which one or two walls are coated with various porous media. The specific objectives of the proposed project, described below, are aimed at testing this hypothesis and achieving our objective of developing and experimentally validating a new

theoretical framework to model and understand this flow and the causes of instability in the system as follows.

1. To develop analytical model for base state (unperturbed) flow of suspensions flows of non-Brownian, non-colloidal particle-laden liquids at moderate to high concentrations (i.e., $0.05<\phi_{bulk}<0.5$) in which one or two walls is/are coated with various porous media.
2. To develop perturbed solutions and eigenvalue problems by linear stability analysis of item 1.
3. To experimentally validate the base-state solutions with the PIV/PTV and MRI measurements.
4. To perform experiments and examine the onset of instability.
5. Compare theoretical/numerical simulations with the experimental data and update the outcomes.

Using the model developed herein, we examined and characterized suspension flows and instabilities in the Taylor-Couette flow system for the first time. Flow and instabilities of Rayleigh-Benard convection flows of suspensions have also been studied. Both results have been published in the Journal of Fluid Mechanics. In addition, we studied the flow in turbulent regime over porous structures using high-fidelity direct numerical simulation and immersed boundary method (IBM) in collaboration with Prof. Luca Brandt at KTH. We have also published these results in the Journal of Fluid Mechanics. The following sections describe these items/outcomes in greater detail.

2. Linear stability analysis for the motion of suspensions over porous media

We consider a fully-developed incompressible flow of a Newtonian fluid (with density ρ and dynamic viscosity μ) driven by a constant pressure gradient in a channel with porous walls (Figure 2). The walls are both homogenous and isotropic and have identical thickness H, porosity ϵ, and permeability κ. They are separated by a distance $2L$ and their outer surfaces are covered by rigid, impermeable plates. The fluid carries spherical solid particles of radius a and density ρ_p.

Assuming a dilute suspension of particles whose size are smaller than the characteristic scale of the flow, we adopt the Eulerian model proposed by Saffman [51] to describe its dynamics in the free-flow layer between the porous walls. The motions of particles are characterized by their number density field n and velocity field $\mathbf{u}_p$. The dynamical coupling of the continuous and particles phases are assumed to be fully represented by the Stokes drag force $\boldsymbol{F}_{St} = 6\pi\mu a(\mathbf{u} - \mathbf{u}_p)$, where $\mathbf{u} = (u, v)$ is the velocity of the continuous phase. The omission of other coupling forces, i.e., the lift, added-mass, Archimedes, Magnus, and history forces, can be justified when the particle size satisfies a condition $a/L \ll 1/\mathrm{Re}$, where the Reynolds number Re is based on the velocity scale U of a bulk flow and can be defined as $\mathrm{Re} = \rho UL/\mu$.

The governing equations of the dusty-gas model are given by [51]

$$\boldsymbol{\nabla} \cdot \mathbf{u} = 0 \tag{1}$$

$$\rho\left(\frac{\partial \mathbf{u}}{\partial t} + \mathbf{u} \cdot \boldsymbol{\nabla}\mathbf{u}\right) = -\boldsymbol{\nabla}p + \mu\nabla^2\mathbf{u} - n\boldsymbol{F}_{St} \tag{2}$$

$$\frac{\partial n}{\partial t} - \boldsymbol{\nabla} \cdot \left(n\mathbf{u}_p\right) = 0 \tag{3}$$

$$\frac{4\pi a^3}{3}\rho_p\left(\frac{\partial \mathbf{u}_p}{\partial t} + \mathbf{u}_p \cdot \boldsymbol{\nabla}\mathbf{u}_p\right) = \boldsymbol{F}_{St} \tag{4}$$

Equations (1) and (2) are the continuity and momentum equations for the continuous phase. The particle transport is described by Eq. (3) and the momentum of the particle phase is given by Eq. (4) where shear diffusion has also been omitted.

The suspension dynamics in the free-flow layer is coupled with the flow dynamics in the porous layers. In this study, the Volume-Average Navier-Stokes equations inside the porous media. For isotropic porous media with negligible fluid inertia and large-scale separation, the equations are hence given by:

$$\boldsymbol{\nabla} \cdot \mathbf{u}_{m,j} = 0, \quad j = 1,2 \tag{5}$$

$$\frac{\rho}{\varepsilon}\frac{\partial \mathbf{u}_{m,j}}{\partial t} = -\boldsymbol{\nabla} p_{m,j} + \mu_e \nabla^2 \mathbf{u}_{m,j} - \frac{\mu}{\kappa}\mathbf{u}_{m,j}, \quad j = 1,2 \tag{6}$$

where $\mathbf{u}_{m,j} = (u_{m,j},\ v_{m,j})$ and $p_{m,j}$ are the velocity and pressure fields in the porous region. The subscript j indicates the upper (j = 1) and lower (j = 2) porous layers. The effective viscosity μ_e takes a value of the order of μ/ϵ so that we will assume $\mu_e = \mu/\epsilon$ throughout the present work for simplicity. The particles are assumed to adhere quickly to pore walls once they enter the porous media. Therefore, no dynamical effect of the particles on the fluid flow is present in the porous walls.

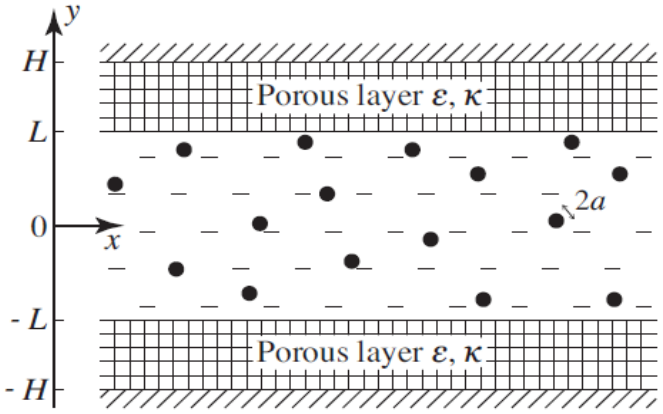

Figure 2. Sketch of the computational domain and coordinate systems.

The governing equations (1)–(6) are supplemented by boundary conditions. At the solid plates, the no-slip conditions are to be satisfied as

$$u_{m,1} = 0, \qquad y = +(H + L); \qquad u_{m,2} = 0, \qquad y = -(H + L). \tag{7}$$

At the surfaces of the porous walls the velocity and normal stress continuities and shear

jump conditions connect the flow dynamics in the free-flow layer and that in the porous layers

$$u_{m,1} = \mathrm{u},\ p - 2\mu\left(\frac{\partial v}{\partial y}\right) = p_{m,1} - 2\mu_e\left(\frac{\partial v_{m,1}}{\partial y}\right), \mu_e\frac{\partial u_{m,1}}{\partial y} - \mu\frac{\partial u}{\partial y} = -\frac{\tau\mu u_{m,1}}{\sqrt{\kappa}},\ \text{at } y{=}L \qquad (8a)$$

$$u_{m,2} = \mathrm{u},\ p - 2\mu\left(\frac{\partial v}{\partial y}\right) = p_{m,2} - 2\mu_e\left(\frac{\partial v_{m,2}}{\partial y}\right),\ \mu_e\frac{\partial u_{m,2}}{\partial y} - \mu\frac{\partial u}{\partial y} = -\frac{\tau\mu u_{m,2}}{\sqrt{\kappa}},\ \text{at } y{=}{-}L \qquad (8b)$$

The coefficient τ represents the stress transfer between the solvent and the porous media and takes different values (zero, positive or negative), depending on the manner in which a porous material's structure varies in the heterogeneous transition layer and on the surface machining of the interface.

2.1. Base sate (unperturbed solutions)

The considered system is invariant to any translation along the channel direction. When the pressure gradient driving the flow is small and thereby, no hydrodynamic instability does not occur, a laterally uniform flow will develop. The velocity profiles of this base state is determined by solving the governing Eqs. (1) – (6) together with the boundary conditions (7) & (8) for steady one-dimensional fields: $\mathbf{u} = U(y)\mathbf{e}_x$, $\mathbf{u}_p = U_p(y)\mathbf{e}_x$, and $\mathbf{u}_m = U_{m,j}(y)\mathbf{e}_x$, where $\mathbf{e}_x$ is the unit vector in the x-direction.

Figure 3 (a) shows the base velocity profiles for different values of momentum transfer coefficient τ while $\epsilon = 0.6$, $H/\sqrt{\kappa} = 50$, and $L/H = 1$. By increasing τ, more momentum transfers from the free flow region to the porous layer resulting in increasing of both free flow and porous layer velocity values. Due to this increase of the slip velocity with τ, the profile of U is shifted slightly to the right with τ, keeping its parabolic shape. The fluid motion is weak in the porous layers except within Brinkmann layers on the fluid-porous interfaces of a thickness of the order of $\sqrt{\kappa/\epsilon}$, where the pressure gradient is balanced with Brinkman's Laplacian force term. The slip velocity is characterized completely by specifying the values of three dimensionless groups: $H\sqrt{\epsilon/\kappa}$, $\sqrt{\epsilon}\tau$, and $L\sqrt{\epsilon/\kappa}$, once it is normalized as $\mu u_s/\kappa G$(u_s is the slip velocity). Indeed, even though u_s involves seven parameters (κ, G, μ, ϵ, L, H, τ), its dependence on them occurs only through these dimensionless groups (The constant G represents the applied pressure gradient). Figure 3 (b) & (c) summarizes the behavior of u_s for two different values of $L\sqrt{\epsilon/\kappa}$. In both cases, the slip velocity does not vary with the momentum transfer coefficient τ when $H\sqrt{\epsilon/\kappa} \ll 1$. In contrast, for large values of $H\sqrt{\epsilon/\kappa}$, it varies sensitively with $\sqrt{\epsilon}\tau$, while $u_s$becomes insensitive to the porous layer thickness (i.e., to the parameter $H\sqrt{\epsilon/\kappa}$).

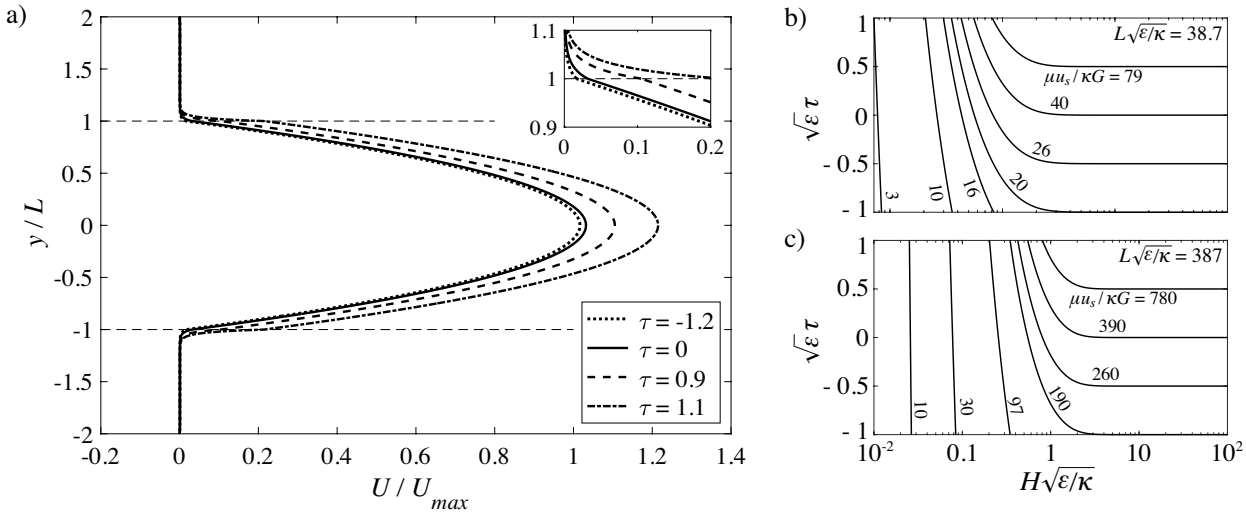

Figure 3. Base state results. (a) The base velocity profiles for different values of the momentum transfer coefficient τ. The other parameters are fixed as ϵ = 0.6, $H/\sqrt{\kappa}$= 50, and L/H = 1. Contours of a normalized slip velocity $\mu u_s/\kappa G$ shown in the parameter space ($H\sqrt{\epsilon/\kappa}$, $\sqrt{\epsilon}\tau$) for two different values of $L\sqrt{\epsilon/\kappa}$: (b) 38.7, and (c) 387.

The velocity fields are independent of the particle density $n = N$ in the base state. In laterally uniform stationary states of flows, the Stokes drag should vanish according to the particle momentum Eq. (4). It follows that the dynamics of the continuous phase is decoupled from the particle dynamics. Any scalar field whose gradient is perpendicular to the flow direction, i.e., $\nabla N \perp \mathbf{u}$, can be a solution for N according to Eq. (3). In the present paper, we will assume that the base particle density N is given by a prescribed constant N_0.

2.2. Linear Stability

To investigate the linear stability analysis of the coupled flow, we first introduce small perturbations. Then linearize the governing equations (1)–(6) around the base state. Also, the boundary conditions (equations (7) and (8)) should be linearized.

Here, we have also nondimensionalized the lengths, the velocities, the time, the pressures, and the particle number density by L, U_{max}, L/U_{max}, ρU^2_{max}, and N_0, respectively and introduced the following dimensionless numbers

$$Re = \frac{\rho U_{max} L}{\mu} \qquad \alpha = \frac{L}{\sqrt{\kappa}} \qquad \delta = \frac{H}{L} \qquad f = \frac{4\pi a^3 \rho_p N_0}{3\rho} \qquad S = \frac{2\rho_p}{9\rho}\left(\frac{a}{L}\right)^2 \tag{9}$$

where Re is the Reynolds number based on the nominal maximum velocity U_{max}, α is the permeability parameter, and δ is the depth ratio. The parameter S is the ratio of the relaxation time associated with the Stokes drag to the viscous diffusion time, $\rho L^2/\mu$. The bulk mass fraction f is identical to the bulk volume fraction of particles, as the particles are assumed neutrally buoyant in the present study. Throughout the present work, we assume small particle volume fractions and small particle radius as $f \ll 1$ and $a/L \ll 1/Re$ for the validity of the dusty-gas model.

2.3. Results and Discussion

Figure 4(a) represents the effect of both permeability and mass fraction f on the neutral curve when $S = 5 \times 10{-}5$, $\delta = 1$, $\epsilon = 0.6$, and $\tau = 0$. As can be observed infinitesimal perturbations grow exponentially and exhibit mono- and multi-modal behavior of the stability for both large and small values of α, respectively. As permeability increases (by decreasing α) the flow destabilizes. In addition, the resulting critical Reynolds number Re_c and wavenumberκ_c, which provide the global minima of the neutral curves, show significant effects of the porous layers on the stability of the channel flow [Fig. 4(b), (c)]. Meaning that as permeability decays for $f = 0.05$, the critical Reynolds number, shown in Fig. 4(b), increases to a value of approximately 4400 that is expected to eventually reaches the corresponding value of Poiseuille flow without particles. Also, by decreasing the porous layer permeability for $f = 0.05$, the critical wave number, illustrated in Fig. 4(c), decreases from 1.34 at the maximum value of α. The particle mass fraction f has a stabilizing effect and adding more particles results in instability thresholds larger than the single-phase flow case, while this effect is not significant for the porous layer of higher permeability ($\alpha \lesssim 240$). In addition, the increase of Re_c and the decrease of κ_c as a function of α is less significant for large particle concentrations than for small concentrations.

On the other hand, particle inertia also affects stability. Fig. 4(d) represents the effect of both permeability and relaxation time S on the neutral curve for $f = 0.05$, $\delta = 1$, $\epsilon = 0.6$, and $\tau = 0$. When the inertia is small ($S = 1.0{\times}10{-}7$), as expected the particles follow the motion of the fluid. Consequently, the particles' presence has no effect on the dynamics of the fluid, while adding more particles leads to lowering the critical Reynolds number. The stability of the suspension channel flow is then identical to the stability of a pure fluid flow driven by the same pressure gradient, while particle inertia stabilizes the base flow. This stabilization is significant for porous layers of small permeabilities, i.e., at large α [Fig. 4(d)]. When permeability decreases for $S = 1.0{\times}10^{-7}$, the critical Reynolds number increases [Fig. 4(e)] and eventually its value approaches to the corresponding value for the plane channel flow without particles. In other words, the decrease of the critical wavenumber as a function of α is more significant when the particle inertia is large [Fig. 4(f)].

From Fig. 5(a), we observe that the amplitude of wall-normal velocity perturbation $|v|$ for a point on the long-wave-branch (i.e., $\kappa = 0.3$) is zero at the channel centerline with a peak at y= ±0.613, then decreases until it vanishes at the walls. Such variation results in the generation of fluid streamlines with two sets of symmetrical vortices, as shown in Fig. 5(b). Although, the existence of fluctuations in $|v|$ due to flow reversal causes the occurrence of small and weak cells within a thin region across the interfaces. Moving to the short-wave branch, i.e., κ=1.3541, Fig. 5(c) shows that the amplitude of wall-normal velocity perturbation peaks at the centerline and then monotonically decays to zero at the walls. As a result, the corresponding streamlines shown in Fig. 5(d) exhibit a single set of periodic vortices in the streamwise direction.

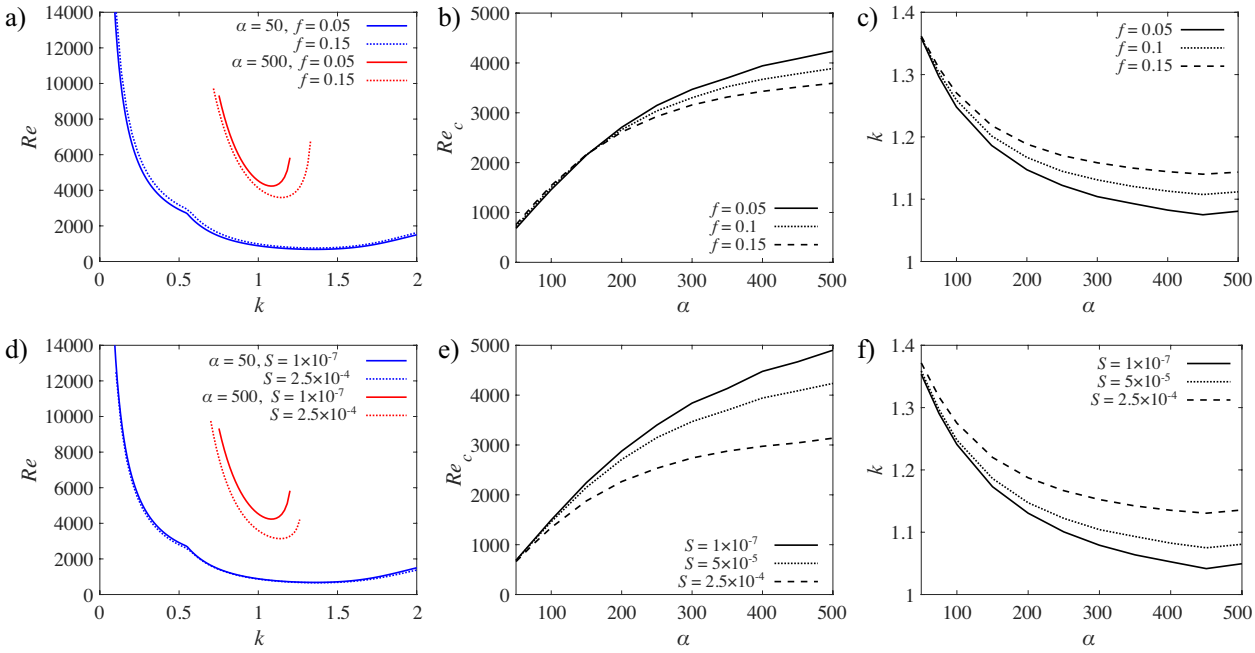

Figure 4. Linear stability behavior as a function of dimensionless parameters. Marginal stability curves for different α and (a) mass fraction f, when $S = 5 \times 10^{-5}$, (d) relaxation time S, when $f = 0.05$. Variation of critical Reynolds number Re_c with α and (b) f, when $S = 5 \times 10^{-5}$, (e) S, when $f = 0.05$. Variation of critical wavenumber κ_c with α and (c) f, when $S = 5 \times 10^{-5}$, (f) S, when $f = 0.05$. For all cases $\delta = 1$, $\epsilon = 0.6$, and $\tau = 0$.

The different flow structures in the two wave-branches might indicate a mode switch in the flow stability. We, therefore, plotted the eigenvalue spectrum for each branch to examine the behavior of eigenvalues, see Figs. 5(e) – (f). In general, the eigenvalues display a Y-shaped structure where the upper left branch is the so-called interface mode since the eigenfunction v vary mostly near the interfaces and is expected to be affected the most by the porous layers, the left branch is called the center mode due to variation of eigenfunctions near the channel center line. The eigenmodes on the near-vertical line in the spectrum diagrams are highly damped waves. It can be seen that the two leading eigenvalues, labeled 1 and 2, belong to the interface mode in both cases. At $\kappa = 0.3$, mode 2 with a greater phase speed $c_i = 0.4638$ dominates the stability; however, as the wavenumber increases to $\kappa = 1.3541$, a mode shift occurs and mode 1 with a smaller phase speed $c_i = 0.4638$ takes over to control the stability. A comparison of flow structures reveals that when mode 2 is leading, the instability causes flow throughout the porous layers and free-flow region (Figs. 5(a) – (b)), whereas mode 1 dominates, causing perturbations mainly inside the free-flow region (Figs. 5(c), (d)). Thus, we can conclude that the onset of instability in porous layers is shifted to the free flow region by moving from the long-wave branch to the short-wave branch. It should be noted that the eigenfunctions of mode 2 are anti-symmetric, while the eigenfunctions of mode 1 are symmetric.

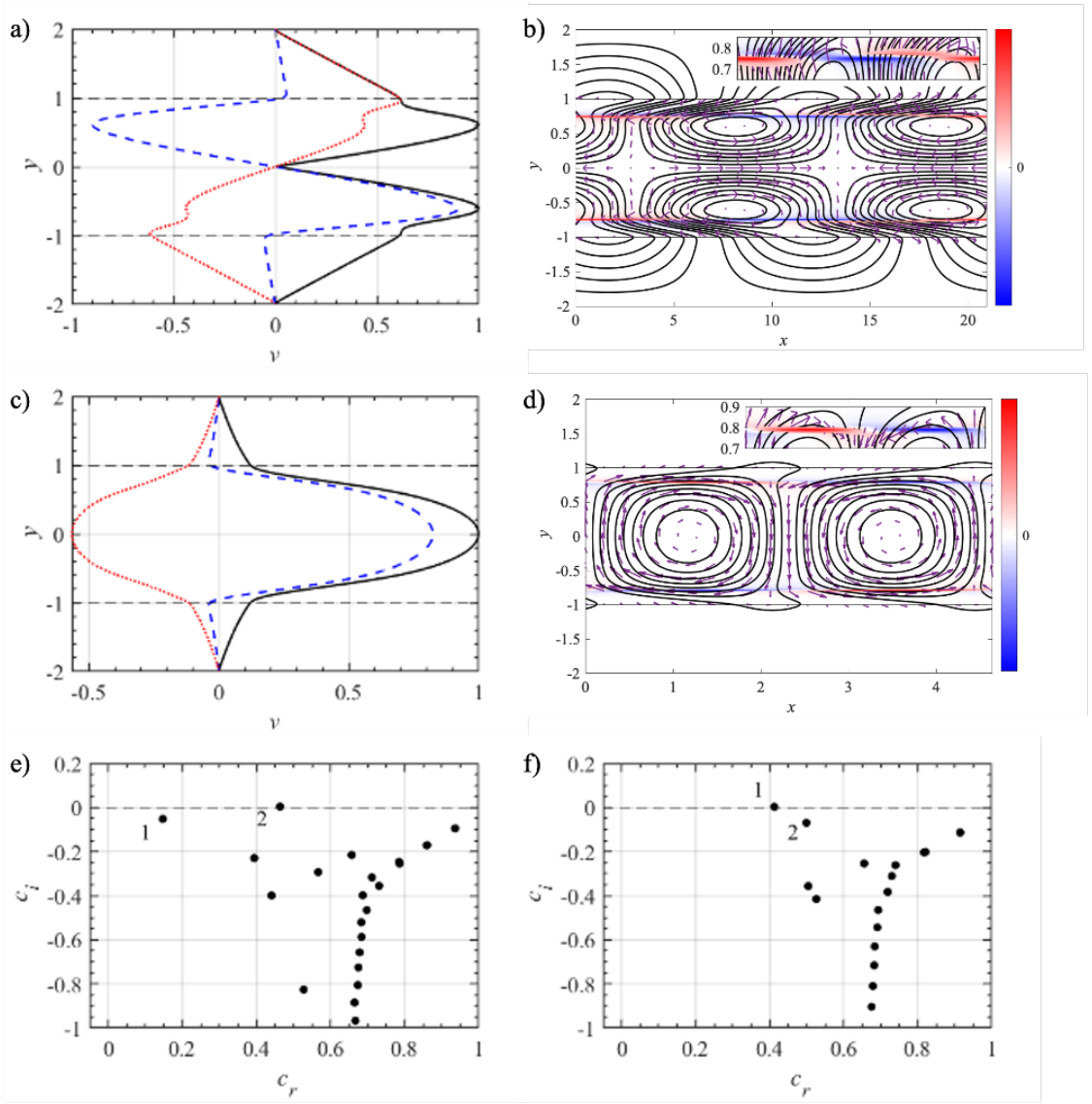

Figure 5. Carrier fluid streamlines and particles distribution contours at (a) $\kappa = 0.3$ and (b) $\kappa = 1.3541$ (global minimum). Wall-normal eigenfunctions, magnitude $|v|$ (black solid lines), real part v_r (blue dashed lines), imaginary part v_i (red dotted lines) of leading eigenvalue at (c) $\kappa = 0.3$ and (d) $\kappa = 1.3541$. Eigenvalue spectrum at (e) $\kappa = 0.3$ and (f) $\kappa = 1.3541$. The Reynolds number are taken as $Re = 1.05 \times Re_c$ at the corresponding wavenumber. For all cases $f = 0.05$, $S = 5\times10^{-5}$, $\alpha = 50$, $\delta = 1$, $\epsilon = 0.6$, and $\tau = 0$.

2.4. Specific Objectives and Key Outcomes of the linear stability analysis of Dusty-gas model over porous media

Although the linear stability analysis of channel suspension flows and pure fluid flow over porous substrates have been extensively investigated previously, the combination of suspension flows over porous media has never been studied before. Here, we have presented the linear stability analysis of uniformly distributed particle-laden flows through a channel where the top and bottom walls are covered with two porous layers.

1. Applying linear stability analysis to find the unstable modes in this new flow system.
2. Validated our model by simulating the particle-laden flows through a channel with impermeable walls as well as particle-less flows between porous media and compared our results with previous works.
3. Finding the effect of particle volume fraction and relaxation time in flow stability when the wall permeability is high, respectively, minor destabilizing and stabilizing effects.
4. Finding the particles and porous walls as flow controllers for maintaining the flow laminar or triggering the transition to turbulence.
5. Analyzing the effect of the momentum transfer coefficient at the porous surface.

These results have been submitted to the Journal of Transport Phenomena. A sample of the manuscript have been added into the "Products/Articles" Section.

3. Experimental methods to validate the base state (unperturbed) solutions using the proposed PIV/PTV and MRI measurements

Next, we examined the base state (steady state or unperturbed) solutions of the particle-laden flows over porous media models. We started with evaluating a dilute suspension containing neutrally buoyant, non-colloidal, non-Brownian, rigid, spherical particles with volume fractions ϕ_{bulk}= 1%, 3%, and 5% when they are passing over and within a porous media model using PIV/PTV and refractive indexed-matching techniques. We were also able to get data for both velocity and concentration profiles for ϕ_{bulk}= 1%, 3%, and 5% suspensions in creeping flow regime (Re<1). Both PIV (2D), PTV, and Shake-the-box (3D) measurements were performed to examine suspensions flows over and through various porous structures. PIV data were collected in two planes, one plane was positioned on top of the rods and another within the rods. The porous media model consists of 3D rigid rods oriented perpendicular to the flow with various porosity ε = 0.7, ε = 0.8, ε = 0.9, and various thickness H = 2mm, H = 3mm, and H = 5mm, resulting in dimensionless permeability parameter, σ = 2.2, σ = 3.46, and σ = 6.09 and dimensionless depth ratio $\delta = 0.74$, $\delta = 1.37$, and $\delta = 4.54$. The outcomes of the PIV measurements have been published and reported in the previous interim reports in [52-54]. The Shake-the-box (3D) measurements results are in preparation to be submitted to the Journal of Physics of Fluids in the near future.

As part of this project and as proposed in the proposal, we also conducted MRI measurements on pure suspending fluid, semi-dilute, and dense concentrated suspensions (i.e., the volume fraction of suspensions ranges from 10% to 40%) in an unperturbed regime. The 3D concentration and velocity measurements were accomplished on a 1 Tesla micro-imaging system with maximum imaging gradients of 400 mT/m, for proton (H1) MRI at Rutgers Molecular Imaging Center (see Figure 6(A)) by collaboration with Dr. Nina C. Shapely. The MRI is computer controlled by a SGI workstation running Aspect Imaging "NRG" software. We used MATLAB and other imaging processing programs such as ImageJ for analysis of acquired data. Figure 6 and Figure 7 represents an example of the calibrated intensity image taken from MRI showing particle distribution and velocity field over and through the porous structure for pure solvent and ϕ_{bulk} =30% suspension at different planes including through the porous media model, at the interface, and inside the free-flow region.

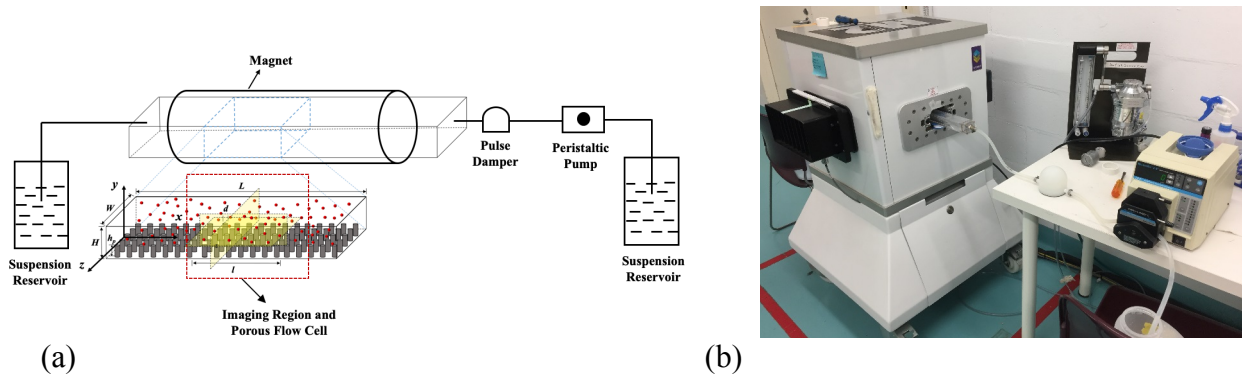

Figure 6. (a) Schematic, and (b) experimental setup for exploring suspension flows over various porous media models using MRI measurements at Rutgers Molecular Imaging Center.

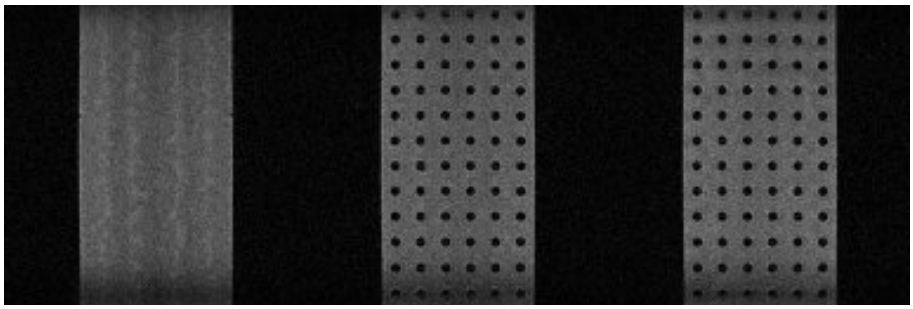

Figure 7. Intensity images showing particle distribution over and through the porous media model for ϕ_b =30% suspension. (a) flow in the free-flow region (y=h_p+ 0.5 mm = 5.5 mm), (b) flow at the suspension-porous interface (y=h_p- 0.5 mm = 4.5 mm), and (c) flow in the middle of the rods (y=h_p-1.5 mm = 3.5 mm). The signal intensity is proportional to the fluid volume fraction, so that low intensity (dark) pixels correspond to high local particle concentration. The length of the flow cross-section (bright region) is 5 cm and the width is 2.5 cm. MRI scan parameters: spin-echo 2D pulse

In particular, Figure 8 shows the particle concentrations distribution in y-z, x-y, and x-z planes for ϕ_{bulk} = 40% suspension flow. These profiles confirm the particle layering in between the rods both inside the free-flow region and inside the rods even for semi-dilute and dense suspensions. Figure 9 also shows the velocity profiles for various suspension concentrations (i.e., ϕ_{bulk} =10%, 20%, 30%, and 40%) in only y-z plane. The velocity profiles show that by adding the particle to the flow the velocity inside the porous structure will dramatically decays. These interesting results lead to insightful knowledge in terms of the motion of particles where the walls are covered with specific porous structure which can lead to new and advanced micro-, bio-fluidic devices. These outcomes also provide information on how to control the flow and particle distribution in channel flows.

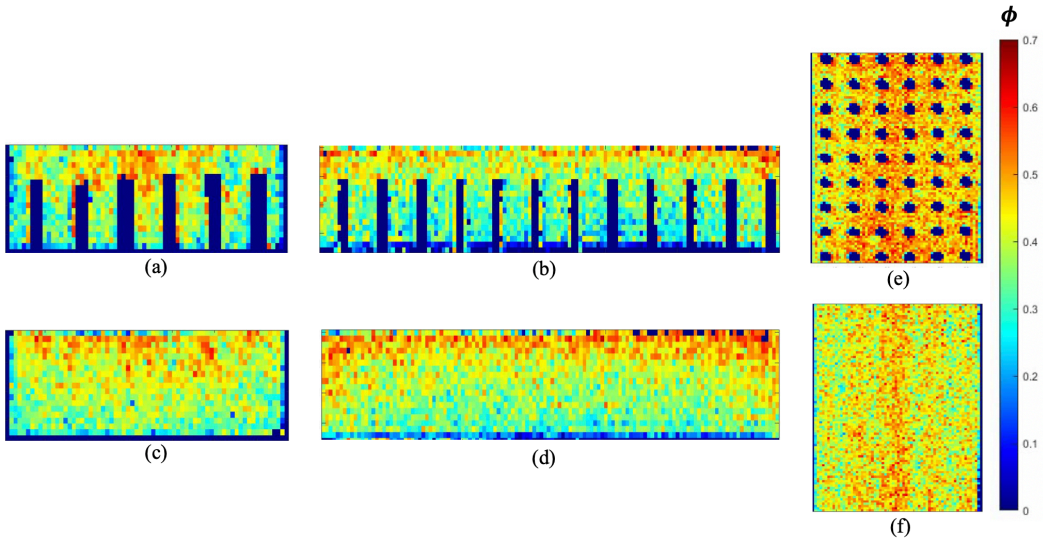

Figure 8. Particle concentration maps for $\phi_b = 40\%$ and Q=70 ml/min, (a) flow on top of the rods and (c) flow in between the rods for front view at (y-z plane at x=23.2 $\pm$ 0.11 cm), height of the flow cross-section (region shown) is 7 mm and the width is 2.5 cm, (b) flow on top of the rods and (d) flow between the rods for side view at (x-y plane at z=0 $\pm$ 0.11 cm), height of the flow cross-section (region shown) is 7 mm and the length is 5 cm, and (e) flow at the suspension-rods interface (x-z plane at y = h_p - 0.5 mm = 4.5 mm) and (f) flow inside the free-flow region for top view at (x-z plane at y=h_p+0.5 mm = 5.5 mm), length of the flow cross-section (region shown) is 3.5 cm and the width is 2.5 cm. MRI scan parameters: spin-echo 2D pulse sequence, TR=2 s, TE=13.7 ms, field of view=5 cm × 5 cm, slice thickness=1 mm,128 × 128 pixels, 1 excitation, scan time=4 min. 16 sec.

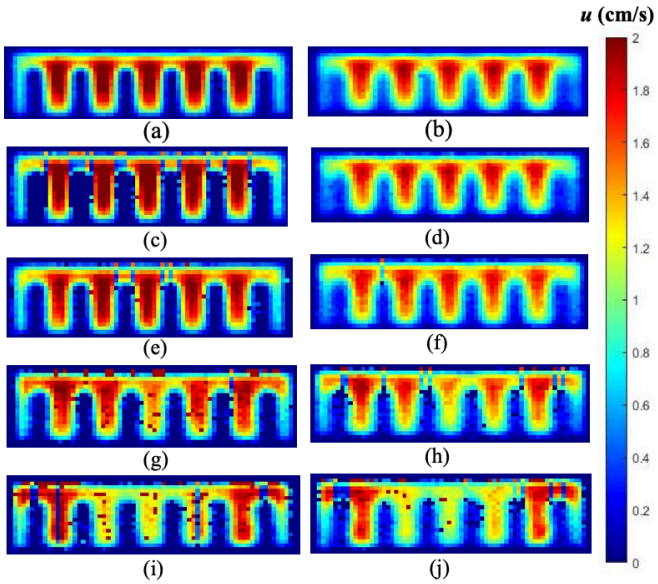

Figure 9. Axial (streamwise) velocity maps (u) (cm/s) viewed in the y-z plane (Q=70 ml/min), for (a,b) pure Newtonian suspending fluid, (c,d) ϕ_b=10%, (e,f) ϕ_b=20%, (g,h) ϕ_b=30%, (i,j) ϕ_b=40%. (a,c,e,g,i) flow on top of the rods, and (b,d,f,h,j) flow between the rods, at distance x=23.2 $\pm$ 0.11 cm after the beginning of the porous medium. The height of the flow cross-section (region shown) is 7 mm and the width is 2.5 cm. MRI scan parameters: spin-echo diffusion weighted imaging pulse sequence, TR=500 ms, TE=23 ms, field of view=5 cm x 5 cm, slice thickness=1 mm, diffusion pulse separation Δ =10 ms, diffusion gradient duration δ =2 ms, diffusion gradient =61.2 mT/m, B value=10, 128 × 128 pixels, diffusion gradients in the slice gradient direction, 1 excitation, scan time=64 sec.

The mean velocity and mean concentration profiles for various suspensions obtained from MRI can be observed in Figure 10 (A, B). Similar to the dilute suspensions and the results obtained using PIV/PTV, the velocity profiles show that by adding more particles to the flow with the existence of the structured surface the velocity inside the porous layer decreases. This is due to the 3D structure of the porous model and the interaction of particles with the rods, resulting in decaying the velocity values within the flow. In addition, as can be seen in Figure 10(B), the concentration profiles obviously specify the particle layering in both the porous model and the free-flow region. It should be noted that when the suspensions are flowing inside smooth/impermeable channel walls, the velocity profile decay by adding the particles resulting in a blunted velocity profile at the center of the channel. Also, due to the shear-induced migration the suspensions migrate to the center where the particle layering cannot be observed.

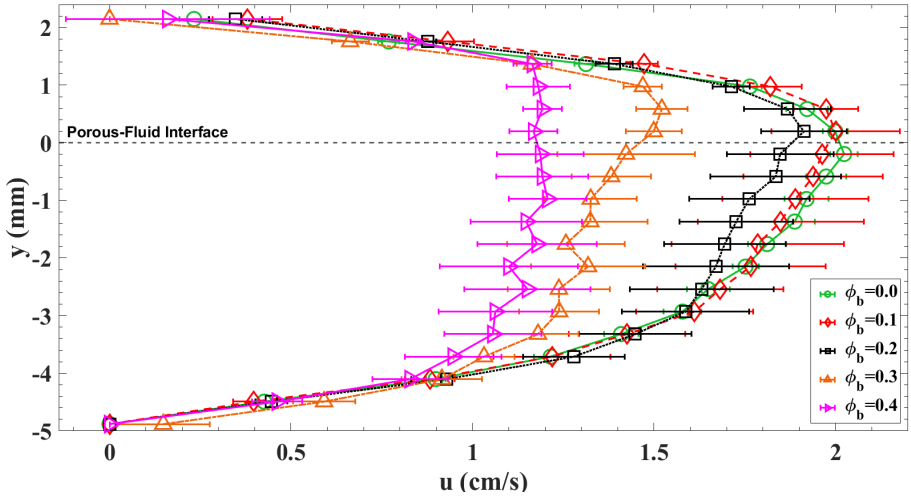

(a)

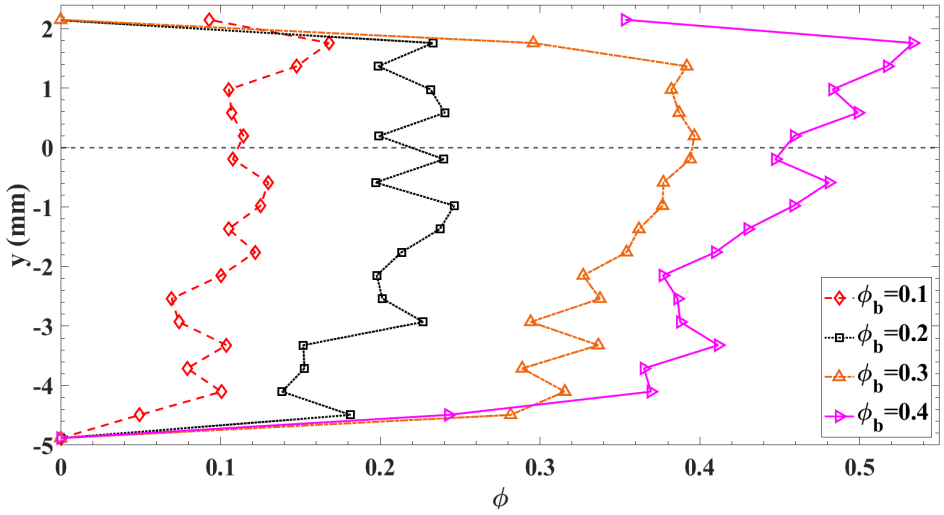

(b)

Figure 10. (a) The mean velocity profiles and (b) Mean particle concentration profiles obtained using MRI over and through the rods of the porous structure for various concentrations ranging from 10% to 40% and Q= 75 ml/min. Data obtained from MRI.

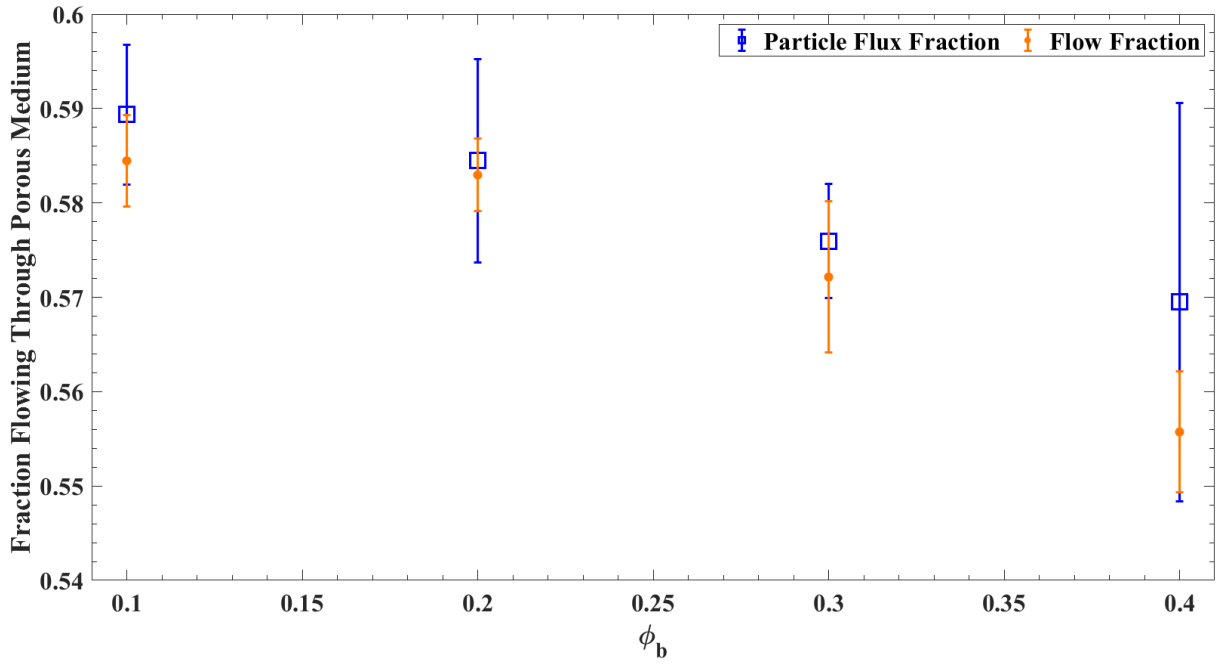

Figure 11. Average flow and particle flux fractions inside the porous model vs. the bulk particle volume fraction, ranging from 10% to 40% for Q=70 ml/min.

To further characterize the suspension flow inside the porous structure, we also plot the average particle flux fraction and the average flow fraction through the porous model for various suspension concentrations and Q=70 ml/min (see Fig. 11). The flow fraction was calculated from the axial velocity maps in Figure 9. The portion of the volumetric flow rate passing through the porous region ($y \leq 0$) was summed over the entire axial cross section and divided by the total volumetric flow rate, for the image on top of the rods and the image between the rods and then the two values were averaged to yield the average flow fraction. The particle flux fraction was calculated from the axial concentration maps in Figure 8. The particle flux in each pixel of the image was calculated by multiplying the local velocity by the local concentration. The portion of the particle flux passing through the porous region ($y \leq 0$) was summed over the entire axial cross section and divided by the total particle flux, for the image on top of the rods and the image between the rods and then the two values were averaged to yield the average particle flux fraction. In general, the flow fraction and particle flux fraction decay slightly, on the order of 5%, as the concentration increases. The data suggest that the flow fraction and particle flux fraction are relatively constant over the examined range of bulk concentrations. Perhaps the observed flow fraction and particle flux fraction correspond to a minimum value of the pressure drop or viscous dissipation. Differences between the particle flux fraction and flow fraction might be due to particle banding at high concentration. It should be noted that porous structure and thickness can impact these results.

3.1. Specific Objectives and Key Outcomes of the PIV/PTV and MRI measurements

The main objective of this project is to study the stability behavior of particle-laden flows in the presence of porous media. However, as mentioned above, the first task is to examine the flow with particles over various porous media models using experiments. The outcomes of this analysis are as follows.

1. While the velocity profiles for low concentrations of suspensions (i.e., 10% and 20%) appear to be similar to those of the pure suspending fluid, as the suspension concentration increases, due to the particle-particle, particle-rod, and particle-wall interactions, the velocity profile is modified.
2. At higher bulk particle concentrations of 30% and 40%, we observe nonuniform particle distributions due to the action of shear-induced particle migration.
3. Particle concentration is enhanced in the free-flow region above the porous medium and reduced at the bottom of the rods in the porous medium.
4. *One of the critical outcomes of this study is the particle banding effect due to the existence of gaps between columns of rods in the porous media model.*
5. It appears that the surface structure leads to the migration of particles to specific locations, leading to banding, in the vicinity of the free-flow region, especially as the volume fraction increases. This impact depends on various parameters including the suspension properties, particle size and shape, and also the thickness and the properties of the porous structure.

The MRI results have been accepted to be published in the Journal of Rheology in Feb. or March 2023. The paper is already archived and a sample of the paper has been also added into the "Products/Articles" Section.

After examining the suspension dynamics and their behavior over and through the porous media using both PIV/PTV and MRI measurements, we compared our data with predicted suspensions continuum models such as diffusive flux model (DFM) proposed by [19]. In our numerical analysis, we coupled 2D DFM to model the suspension flow with the volume-averaged Navier-Stokes (VANS) equations in the porous media. Figure 12(a) shows the velocity profile for various dilute suspensions and their comparison with the analytical results (i.e., DFM). It can be seen that there is good agreement between all profiles within the free-flow region. However, the experimental results show much lower velocities within the porous media. Also, the porous velocity is even lower at the higher concentrations, which supports the idea that the particles within the flow are interacting with the rods of the porous media. Furthermore, this discrepancy could be due to the 3D impact of the experiments while the analytical model is 2D. Figure 12(b) represents the comparison of the MRI obtained concentration data with the DFM. The discrepancy between the experimental and theoretical results is obvious, where the model cannot properly capture the layering effect of the particles with the existence of the suspensions in the flow. In addition, because the model does not consider the motion of particles inside the porous region, the suspension flow inside the region is zero.

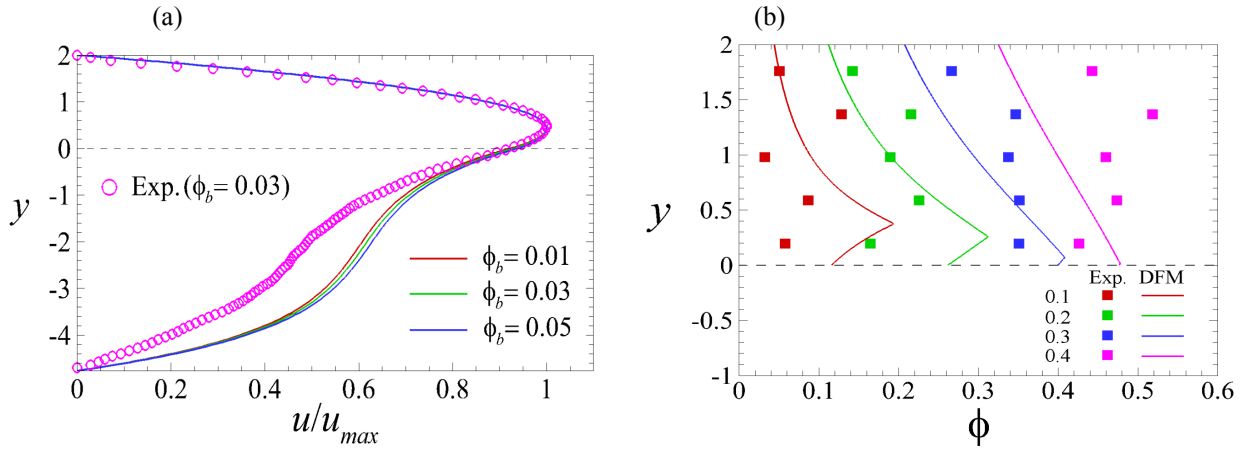

Figure 12. (a) The averaged velocity profiles, and (b) the mean concentration distribution from the PIV/PTV and MRI measurements and their comparison with the diffusive flux model (DFM). Experimental study (data points) compared to the results from the DFM (solid lines).

Since we found some discrepancy between the experimental and DFM results. As mentioned above, this might be due to the fact that the DFM is a continuum 2D model that does not capture the particles size, their collision and their interactions with the porous surface properly. We then integrated a 3D fully resolved, high-fidelity numerical method including both DNS and IBM by collaborating with Prof. Luca Brandt (KTH, Sweden) to resolve these issues. The novelty of this task lies in the coupling of the suspension dynamics with the porous medium approaches as follows.

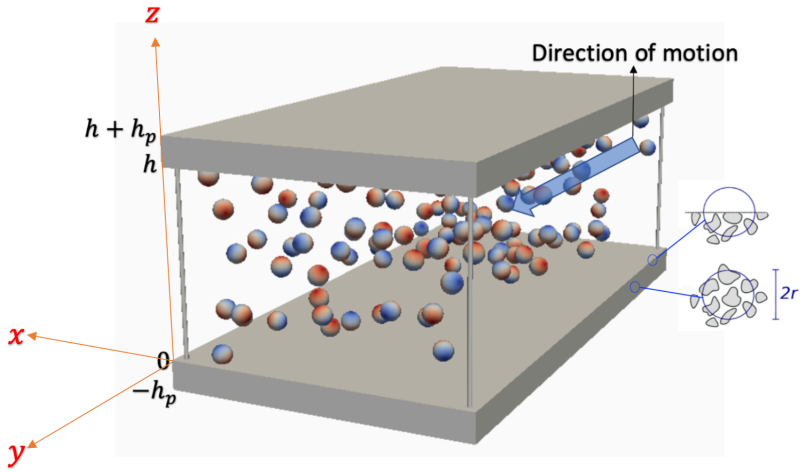

Figure 13. Sketch of the suspension flow in a channel with the existence of porous layers on both sides of the channel for $\phi_{bulk} = 10\%$.

We considered a flow of an incompressible viscous fluid in a channel. x, y and z (x_1, x_2, $and x_3$) denote the streamwise, wall-normal and spanwise coordinates, respectively, while u, v and w (u_1, u_2, u_3) denote the corresponding components of the velocity vector field as shown in Figure 13. Rigid spheres, with the same mass density as the carrier fluid and size R, are suspended in the purely fluid region between the two porous slabs. In the continuum limit, the flow of an incompressible viscous fluid through the whole domain, which includes the porous layers is

governed by the Navier-Stokes equations. In particular, the motion of the fluid is governed by the conservation of momentum and the incompressibility constraint defined as

$$\rho\left(\frac{\partial u_i}{\partial t}+\frac{\partial u_i u_j}{\partial x_j}\right)=\frac{\partial \tau_{ij}}{\partial x_j} \quad \text{and} \quad \frac{\partial u_i}{\partial x_i}=0 \tag{10}$$

Here, ρ indicates the fluid density and τ_{ij} the Cauchy stress tensor. The fluid is assumed to be Newtonian with constitutive equations $\tau_{ij}^{f}-p\delta_{ij}+2\mu D_{ij}$, where p is the pressure, μ is the fluid dynamic viscosity, D_{ij} is the strain rate tensor defined as $D_{ij}=\left(\frac{\partial u_i}{\partial x_j}+\frac{\partial u_j}{\partial x_i}\right)/2$ and δ is the Kronecker delta. The particle motion (velocity and rotation) is governed by the Newton-Euler equations, stated as

$$\rho^p V^p \frac{dU_i^{pc}}{dt}=\oint_{\partial V^p}\tau_{ij}n_j dA+F_i^c,\; I^p\frac{d\Omega_i^p}{dt}=\oint_{\partial V^p}\epsilon_{ijk}r_j\tau_{kl}n_l dA+T_i^c \tag{11}$$

where ρ^p, I^p and V^p are the particle density, moment of inertia and volume. In particular, for rigid spheres with radius R^p, we have $V^p=\left(\frac{4}{3}\right)\pi {R^p}^3 and\ I^p=(2/5)\rho^p V^p {R^p}^2$. In the previous equations, τ_{ij} is the fluid stress tensor reported in equation (10), n_j is the unit normal vector pointing outwards from a particle and F_i^c and T_i^c are the force and torque acting on the particles due to particle-particle and particle-wall interactions.

The presence of a rigid particle is considered with an immersed boundary method (IBM) by introducing an additional body force f_i on the right-hand side of the momentum equation in equation (10) that forces the fluid velocity on the particle surface to match the particle velocity. The interactions between the particles or with a wall are taken into account using a lubrication correction and a soft collision model; when the thin gap distance between two approaching particles (or between particle and wall) becomes less than a certain threshold, lubrication correction models based on Brenner's asymptotic solution are employed to correctly reproduce the interaction between the particles.

We then characterized the porous layer by considering its porosity ε and the permeability K_{ij}. The flow of an incompressible viscous fluid through porous layers within a porous medium is also governed by the Navier-Stokes equations with the imposition of no-slip boundary conditions on the porous elements. The volume-averaged Navier-Stokes equations can be defined as

$$\rho\frac{\partial\langle u_i\rangle^s}{\partial t}=-\varepsilon\frac{\partial\langle p\rangle^f}{\partial x_i}+\mu\frac{\partial^2\langle u_i\rangle^s}{\partial x_j\partial x_j}-\frac{\mu\varepsilon}{\mathcal{K}}\langle\tilde{u}_i\rangle^s,\ \frac{\partial\langle u_i\rangle^s}{\partial x_i}=0 \tag{12}$$

where $\tilde{u}_i$ is the difference between the flow and the porous medium velocity, which is set equal to the wall velocity. The previous equations are obtained by introducing two averaging operators over the volume of fluid V_f contained within the elemental porous volume V: the superficial volume average $\langle\psi\rangle^s=1/V\int_{V_f}\psi dV_f$, and the intrinsic volume average $\langle\psi\rangle^f=1/V_f\int_{V_f}\psi dV_f$ (here ψ is any fluid variable). Note that, the first average is linearly related to the second via the porosity, i.e., $\langle\psi\rangle^s=\frac{V_f}{V\langle\psi\rangle^f}=\varepsilon\langle\psi\rangle^f$. Because of the incompressible character of the flow, the superficial

volume average is commonly used for the velocity field, while the intrinsic volume average is preferred for the pressure, being directly related to experimental values.

Our numerical simulations are based on a 3D solver that adopts an IBM for the particles in the purely fluid region $0 < y < h$, while the volume-averaged Navier-Stokes equations (12) are solved in the two porous layers $-h_p < y < 0$ and $h < y < h + h_p$. The set of equations is formally closed by imposing no-slip boundary conditions on the rigid walls, on the rigid porous material surface and on the moving particles. The boundary condition at the interfaces ($y = 0$ and $y = h$.) can be simplified as

$$u_i = \langle u_i \rangle^s,\ p_i = \langle p \rangle^s,\ \frac{\partial u}{\partial y} = \frac{1}{\varepsilon}\frac{\langle u \rangle^s}{\partial y},\ \frac{\partial w}{\partial y} = \frac{1}{\varepsilon}\frac{\langle w \rangle^s}{\partial y}, \tag{13}$$

We considered both Couette flow and pressure-driven flow of a Newtonian fluid laden with rigid spherical particles with radius $R = h/5$. The Reynolds number of the simulation for Couette flow was considered at $Re = \frac{\rho \dot{\gamma} R^2}{\mu} = 0.1$, where $\dot{\gamma} = U_{bulk}/h$ is the reference shear rate; therefore, we can consider inertial effects to be negligible. For the pressure-driven channel flow with the existence of the upper and lower porous walls, the Re was varied from 0.1 to 5600. Two porous layers of thickness h_p and porosity ε move with the wall velocity, and the purely fluid region of the domain is bounded by these layers. The numerical domain has size $8R \times 5R + h_p \times 8R$ and periodic boundary conditions are enforced in the streamwise x and spanwise z directions. We considered three values of the nondimensional permeability $\sigma = \sqrt{K}/h$, covering the range $\sigma \in [0.79 : 7.9] \times 10^{-3}$, all in the small permeability limit due to the hypothesis of negligible inertia inside the porous layers; the impermeable case, $\sigma = 0$, is used as a reference. In most of our simulations, we fix the porous layer thickness to $h_p = h/2$ and the porosity to $\varepsilon = 0.6$; however, we also evaluate the effect of these parameters by simulating selected cases with $h_p = h/4$ and $h_p = h$ and $\varepsilon = 0.3$ and $\varepsilon = 0.9$. Rigid spherical particles are suspended in the purely fluid region of the domain and their volume fraction ϕ_{bulk} is varied in the range $\phi_{bulk} \in [0 : 0.3]$, corresponding to the number of particles N_p particles suspended in the fluid domain ranging from 0 to 183 at $\phi_{bulk} = 0.3$. The outcomes of the Couette flow for Re=0.1 has been already published in *J. Chemical Eng. Science, 2021*. The results for turbulent flows of suspensions over porous media are in press in the *J. Fluid Mechanics* (a sample of the paper has been added to the "Products/Articles" Section).

3.2. Specific Results on fully resolved DNS and IBM coupled with the VANS for porous layer

1. As mentioned before, to reduce the discrepancy between the experimental data and the DFM, we decided to develop a model that can solve, in a computationally efficient manner, the governing equations in the presence of numerous moving particles modeled as individual solids particles. For this purpose, we first examined creeping flow of suspensions (Re=0.1) in a Couette geometry where the results have been published in *J. Chem. Eng*. Last year (2020). To further examine the flow in other regimes, this Year we studied the turbulent suspension flow of mono-dispersed, neutrally buoyant, rigid, spherical particles over porous media in a channel where the particles do not enter inside

the porous layers. Figure 14 presnts the contours of the normalized streamwise velocity component from instantaneous snapshots for the three different volume fractions under investigation. Based on the results, it can be seen that the suspension flow streamwise velocity is sensitive to the particle volume fraction Φ_b. In particular, the turbulence activities are greatly enhanced throughout the channel due to the disturbances from the particles inside the channel. As the particle volume fraction increases, the streamwise velocity increases at the center of the channel; however, the velocity intensity decreases near the interface suggesting that the slip-velocity decreases when increasing the number of particles in the flow.

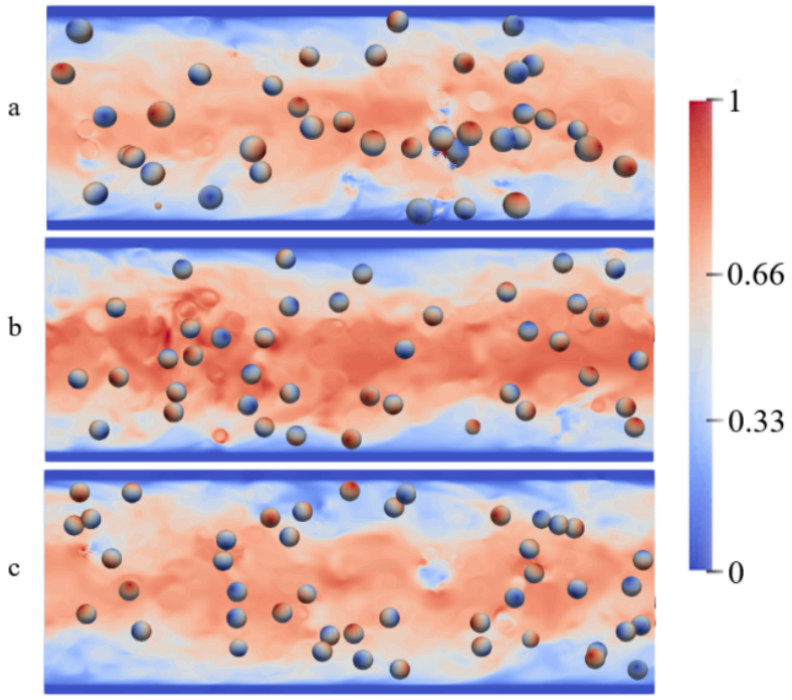

Figure 14. Contours of the instantaneous turbulent streamwise velocity u in the x − y plane for a fixed wall permeability paramter, $\sigma = 0.63 \times 10^{-3}$ and three different particle volume fractions: (a) $\Phi_b = 0.05$, (b) $\Phi_b = 0.1$, and (c) $\Phi_b = 0.2$.

2. Figure 15(a) shows the mean local volume fraction φ for the case of wall permeability paramter $\sigma = 0.63 \times 10^{-3}$ and the three nominal volume fractions Φ_b investigated, while panels (b-c) display how the particle distribution changes with the permeability for two different values of the particle volume fraction.
   A first local maximum close to the interface is form which is associated with the particle-wall layers in the free-flow region. It is observed that the intensity of the particle wall layer increases as the particle volume fraction increases (see panel (a) of the figure). Its formation is explained by the solid lubrication interactions when a particle reaches the wall, which stabilizes the near-wall particle position; once close to the wall, the motion of finite-size particles is mainly influenced by collisions with other particles. Consequently, it is difficult for particles belonging to the first layer to escape.

In the presence of a permeable wall, a weak migration of particles away from the wall and a less pronounced wall layer for $\Phi_b = 0.05$ and 0.10, with the peak value close to the wall found to decrease with the permeability, consistent with the observation of increased wall-normal fluctuations. It should be noted that these near-wall maxima are on the order of the bulk concentrations and are not related to the turbophoretic drift observed in dilute suspensions of heavy particles [55]. The same trend observed here was reported in [56] for laminar Couette flow of suspensions over a porous substrate. Finally, it is also illustrated an increase in the local volume fraction φ toward the channel centerline for the largest volume fraction examined, $\Phi_b = 0.20$. This migration toward the channel core was observed experimentally in turbulent flows over solid walls and related to inertial effects in [57]. The accumulation toward the centreline was also associated with quenching of the turbulence fluctuations and reduced mixing [58].

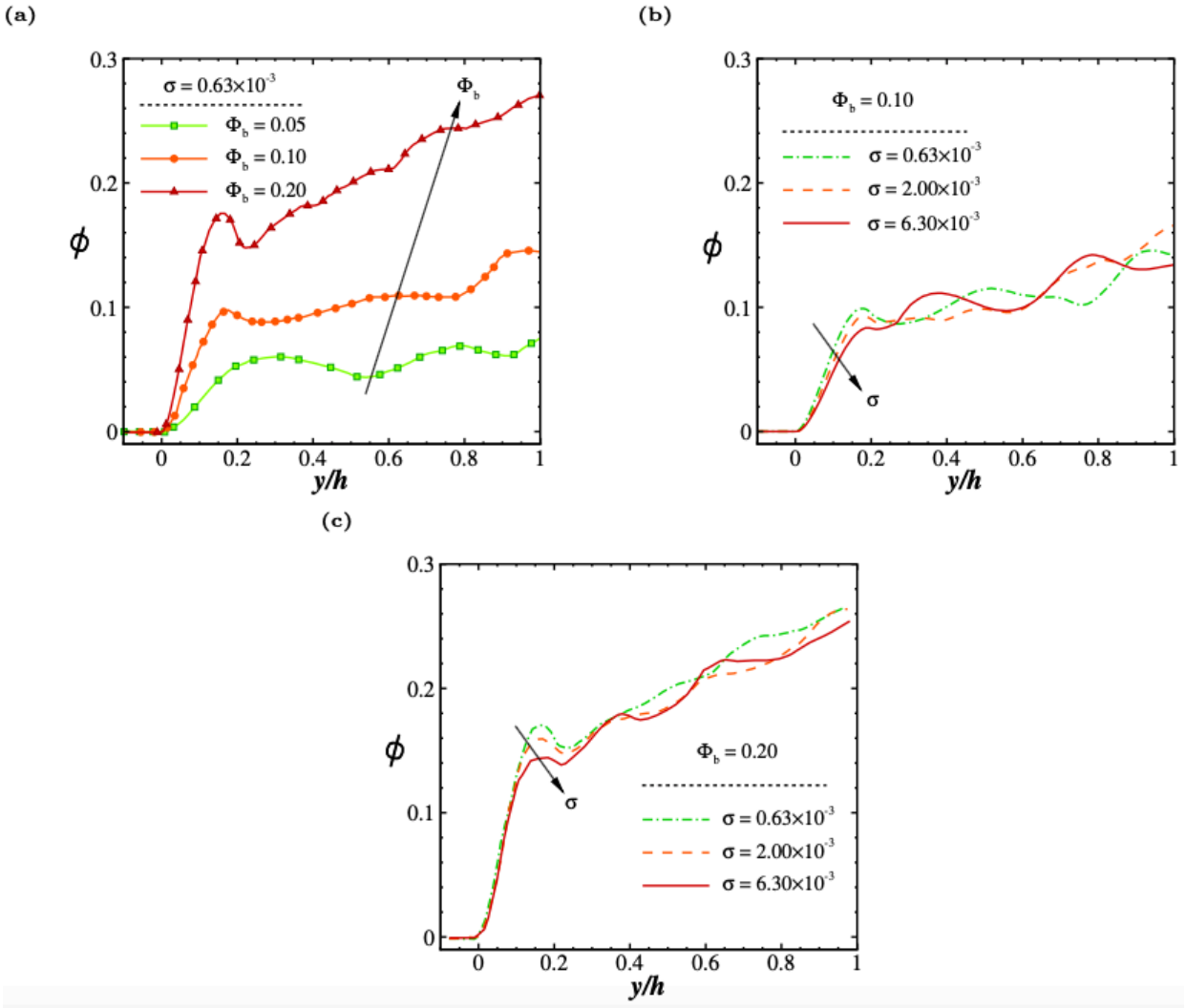

Figure 15. Average particle concentration ϕ as a function of the wall-normal distance y for (a) different particle volume fractions at fixed permeability parameter $\sigma = 0.63 \times 10^{-3}$, (b) and (c) various wall permeabilities σ at fixed particle volume fractions $\Phi_b = 0.10$ and 0.20.

3. The slip velocity u_s at the interface, y = 0, normalized by the bulk fluid velocity is shown in Figure 16(a) for different values of the wall permeability and of the particle volume

fraction. As expected, by increasing the permeability parameter σ, the slip velocity increases, while with increasing particle volume fraction it decreases for all cases studied here. Interestingly, for $\Phi_b \leq 0.10$, the slip velocity is weakly dependent on the volume fraction, and it is mainly determined by the permeability under dilute conditions. Indeed, a more significant variation in the u_s values is observed when further increasing the dispersed phase concentration up to 0.2. These results confirm that the suspension slip velocity in turbulent flows depends on the porous permeability, and when the porous permeabilities are low, i.e., $\sigma = O(10^{-4})$, the slip velocity depends mainly on the suspension concentration. In Figure 16(b), it is characterized the normalized wall-normal velocity fluctuations at the interface for different values of the wall permeability parameter σ and the particle volume fraction Φ_b. Based on the results, the wall-normal velocity fluctuations increase with both the particle volume fraction and the wall permeability, from zero for small wall permeability to the largest value for the highest Φ_b. Note that the velocity fluctuations at the suspension-porous interface do not change significantly with the values of σ investigated; instead, the effect of the particle volume fraction is more pronounced with a more significant increase for $\Phi_b = 0.2$. By comparing the Figures 16(a) and 16(b), it can be concluded that the mean slip at the wall is mainly determined by the wall permeability, while the velocity fluctuations are significantly influenced by the particle dynamics in the free-flow region.

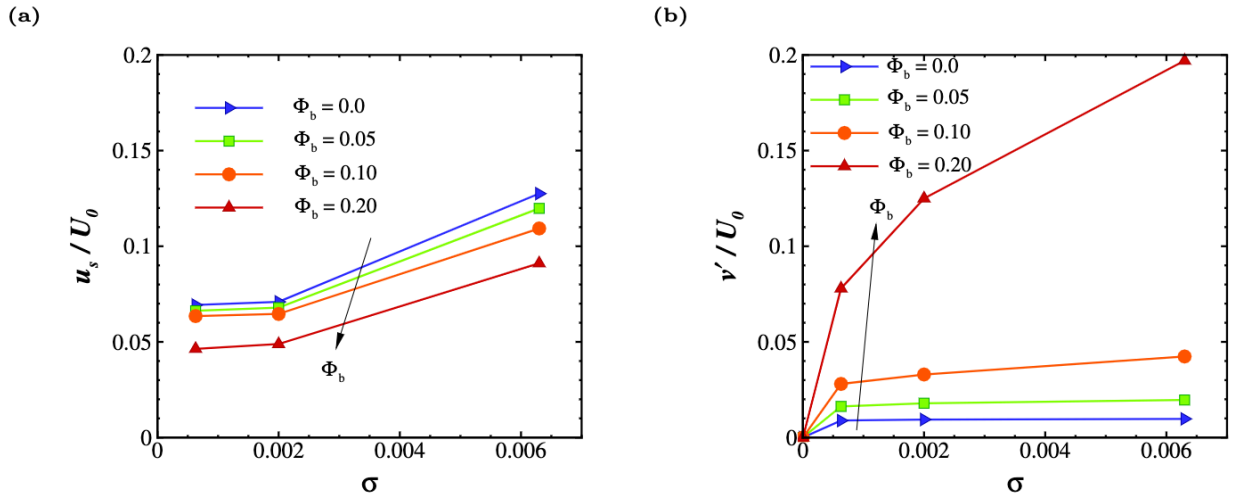

Figure 16. (a) Normalized interface slip velocity as a function of the wall permeability parameter σ for the different particle volume fractions under investigation and (b) normalized interface wall-normal fluctuation velocity as a function of the wall permeability parameter σ for different particle volume fractions Φ_b.

4. In Figure 17(a), the normalized slip velocities for different cases studied here are shown. This figure shows that the slip velocities for nonzero momentum transfer coefficient τ are much smaller than for the case $\tau = 0$ in both single-phase flow ($\Phi_b = 0$) and $\Phi_b = 0.20$. It should be noted that, even for larger permeabilities, previous works observed the same trend for the slip velocity for both positive and negative τ; see, for example, the results for a single-phase flow over porous media in [56]. Figure 17(b) illustrates the normalized spanwise component of the mean particle angular velocity for the different momentum transfer coefficients τ under consideration. Note that the values have been averaged over all particles close to the interface. These data reveal that the particle average angular

velocity decreases significantly for values of the momentum transfer coefficient τ different from zero, consistent with the trend exhibited by the slip velocity.

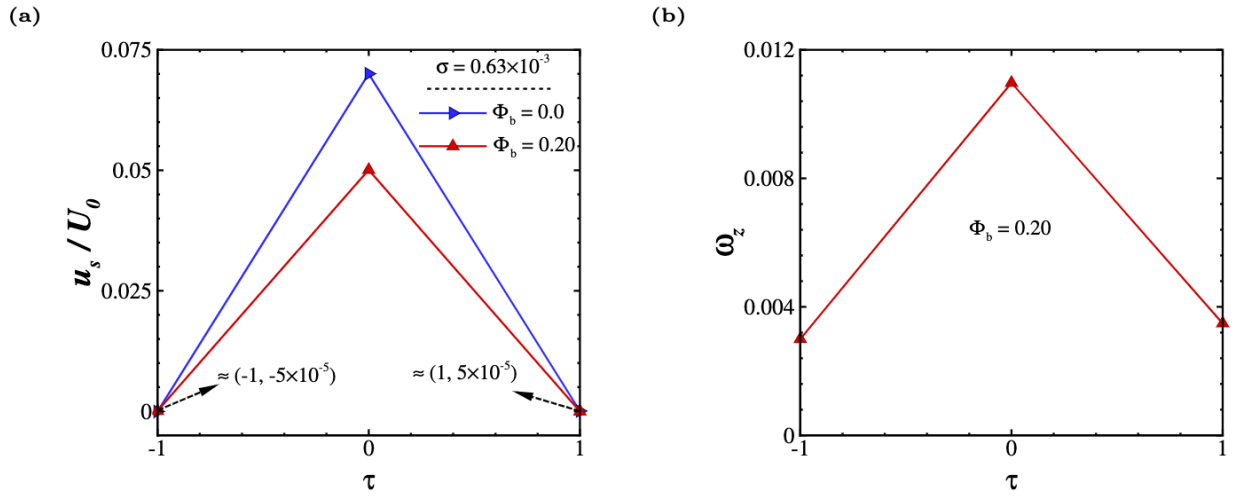

Figure 17. (a) Normalized interface slip velocity as a function of τ for different particle volume fractions under investigation at wall permeability $\sigma = 0.63 \times 10^{-3}$. (b) Normalized spanwise component of the particle angular velocity as a function of τ for particle volume fractions $\Phi_b = 0.20$.

As part of this project, the PI has developed direct numerical simulations (DNSs) and immersed boundary method (IBM) for neutrally buoyant, non-Brownian and non-colloidal, spherical suspensions concentrated in an incompressible Newtonian viscous fluid in the Rayleigh–Bénard (RB) convection. For the very first time we examined the suspensions flow and their behavior in Rayleigh–Bénard (RB) convection and characterized flow regimes of suspension flows. The outcomes will impact many physical phenomena such as heat transport in stars, atmospheric flows and oceanic currents. These results are just *published* in the Journal of Fluid Mechanics (Manuscripts has been added into the "Products/Articles" Section. Some of the outcomes are summarized below.

3.3. Specific Results on numerical simulations of various suspensions ranging from 10% to 40% in a turbulent Rayleigh–Bénard convection

1. Turbulent thermal convection characterizes many physical phenomena such as heat transport in stars, atmospheric flows and oceanic currents. The most commonly studied configuration resembling these flows is the Rayleigh–Bénard convection, i.e., a fluid layer that is heated from below and cooled from above. This simple configuration helped to shed some light on the rich physics of turbulent thermal convection, both in terms of large-scale and small-scale. In this study, the effects of dispersed finite-size particles in turbulent Rayleigh–Bénard convection are quantified. The suspended particles are neutrally buoyant, with all thermophysical properties matching the properties of the fluid.

   Figure 18 shows the three-dimensional (3D) geometry considered for this study. A fluid layer containing the suspended particles is enclosed between two infinitely long horizontal

solid walls, heated from below and cooled from above at a constant temperature at a constant temperature. The x and y directions are considered periodic. The geometry dimensions are defined as (L_x, L_y, L_z) = (2L, 2L, L) where L is the characteristic length used in the dimensionless parameters. A parametric study of the particle volume fraction is carried out, with all other dimensionless parameters considered constant. The particles are considered to have a zero thermal expansion coefficient be (i.e. neutrally buoyant). Other than that, the particles share the same properties with the fluid. The values of the dimensionless parameters adopted along with other numerical parameters are shown in table 1, amounting to a total of nine simulations.

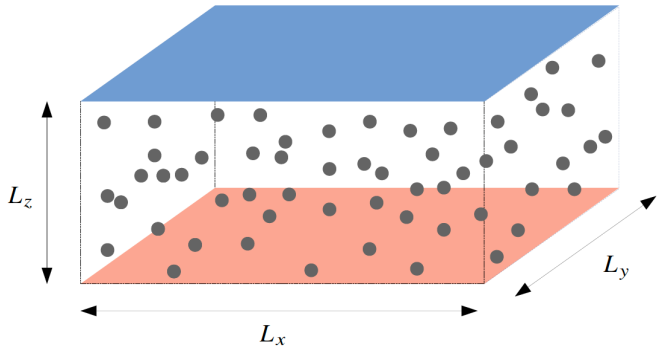

Figure 18. Schematic representation of the set-up used in the present study. The domain dimensions along the x, y and z directions are (Lx, Ly, Lz) = (2L, 2L, L) and the ratio of diameter of the suspended particles is set to d^*_P=1/15. The fluid and the suspended particles are heated from the bottom wall (denoted with red) and cooled from the top wall (denoted with blue).

Ra	Pr	D_p	Φ	$N_x \times N_y \times N_z$	CFL
10^8	7	$L_z/15$	{1, 5, 10, 15, 20, 25, 30, 35, 40}	$960 \times 960 \times 480$	0.5

Table 1: Physical and numerical parameters adopted in the present study.

2. Focusing on the fluid phase, Figure 19 shows two instantaneous temperature iso-surfaces for different values of the particle volume fraction. These iso-surfaces give a better understanding of the structure of the plumes that are ejected from the bottom and top boundary layers. Starting from bulk volume fraction of Φ = 10%, the bottom boundary layer features an active region with intense plume ejection next to a more quiescent region. The same is true for the top boundary layer, with its quiescent region located opposite the bottom boundary layer's active region, and vice versa. This three-dimensional plume configuration facilitates the presence of a large-scale circulation. For particle volume fractions up to Φ = 30%, the presence of a solid phase intensifies the plumes in the quiescent regions. Furthermore, the particle inertia helps the plumes ejected from the active regions to travel through the bulk of the cavity all the way to the opposite boundary layer. By contrast, increasing the particle volume fraction even further, to Φ = 40%, has the

opposite effect; the ejection of plumes is suppressed, without a clear distinction between active and quiet regions and no clear indication of a large-scale circulation structure.

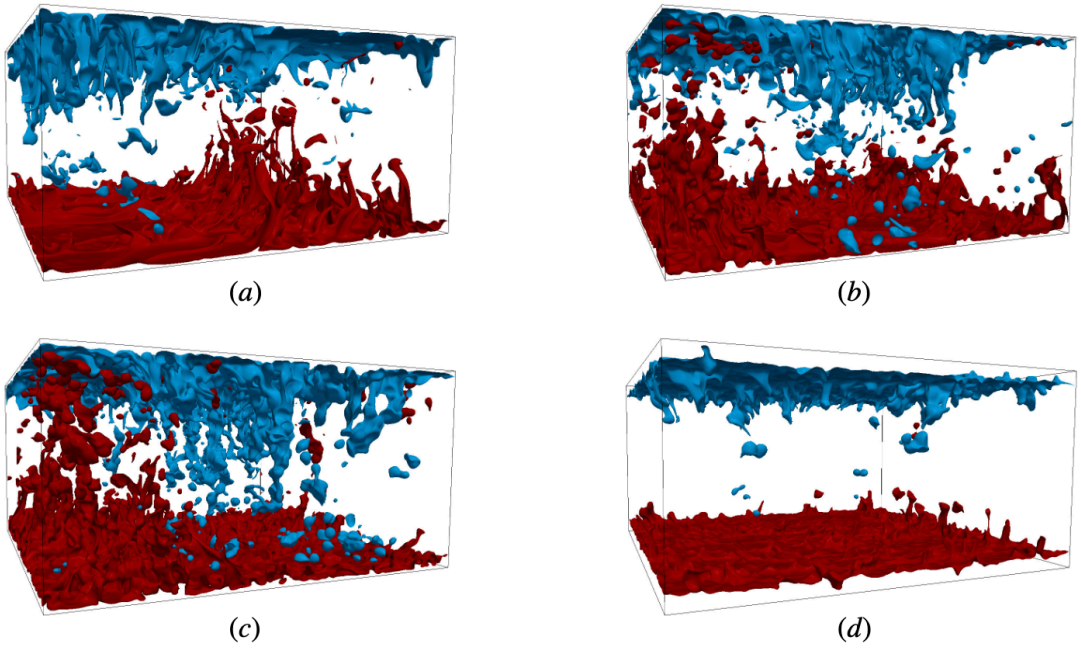

Figure 19. Snapshots of temperature iso-surfaces for (a) Φ = 10%, (b) Φ = 20%, (c) Φ = 30%, and (d) Φ = 40%. In all the cases, the ratio of diameter of the suspended particles d^*_P=1/15. Red color corresponds to T = 0.1 and blue color corresponds to T = −0.1.

3. The heat transfer inside the cavity is expressed through the Nusselt number and shown in Figure 20(a) as a function of the particle volume fraction, for the ratio of diameter of the suspended particles d^*_P=1/15. The Nusselt number is calculated by averaging the heat fluxes at the bottom and top walls. Up to Φ = 25%, the Nusselt number increases almost linearly with the particle volume fraction, reaching a maximum value of 33.8, from 31.8 at Φ = 0%; a relatively mild increase of approximately 6%. Beyond that point, a steep decrease is observed with the Nusselt number dropping to 7.8 for the highest particle volume fraction considered, Φ = 40%. The decrease of the Nusselt number at higher values of Φ is attributed to the decreased mixing due to the particle migration towards the channel core. More specifically, turbulence fluctuations decrease significantly at the centerline where the particles move together as a compact aggregate with reduced relative velocities and rotation rates.
   Another important characteristic of thermal convection is the thermal boundary layer thickness, defined either using the temperature gradient at the wall,

$$\lambda^{\nabla T} = \frac{(\nabla < T > |_{z=0})^{-1}}{2} \tag{14}$$

   or as the location of the maximum rms of the temperature field,

$$\lambda^{rms} = \text{argmax}_z(T^{rms}) \quad (15)$$

where T is the phase averaged temperature. The values of the thermal boundary layer thickness obtained from both definitions are shown in figure 20(b) as a function of the particle volume fractions. As expected from its definition, $\lambda^{\nabla T}$ follows the opposite trend as of the Nusselt number, with a small decrease for moderate particle volume fractions and a steep increase beyond $\Phi = 25\%$. On the other hand, λ^{rms} increases monotonically with the solid volume fraction in the range explored. Starting from slightly different values at $\Phi = 0\%$, the two definitions converge to approximately the same value at $\Phi \approx 20\%$ and retain their agreement for up to $\Phi \approx 35\%$. At the highest volume fraction considered, a large deviation is observed. Even though the temperature gradient at the walls decreases and $\lambda^{\nabla T}$ increases significantly, the maximum temperature rms value does not shift further from the walls, which explains the difference between the two values at the highest particle volume fractions.

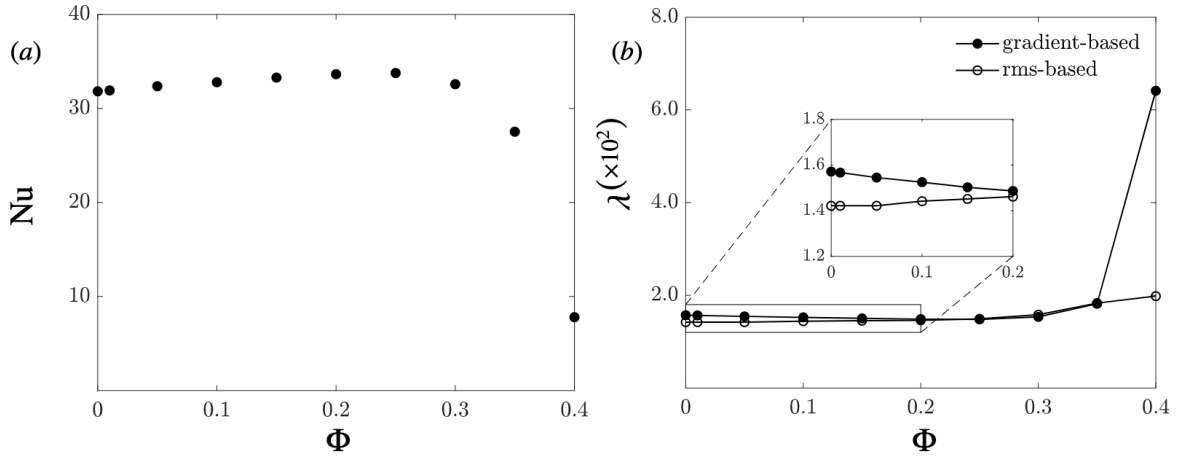

Figure 20. (a) Nusselt number and (b) thermal boundary layer thickness as a function of the particle volume fraction, for d^*_P=1/15. The boundary layer thickness based on the gradient is defined in equation (5) and the rms-based definition given in equation (6). Both quantities are calculated by averaging the relevant quantities at the bottom and top walls.

4. The time- and area-averaged local particle volume fraction $< \varphi >$ as a function of the vertical direction z, shown in Figure 21 for the different values of the nominal particle volume fraction under investigation, and d^*_P=1/15. In all the cases, we see a peak close to the wall, indicating the presence of a layer of particles adjacent to the boundary, while the bulk of the cavity features a homogeneous local volume fraction distribution with $< \varphi > \approx \Phi$. It is also indicated that, as the particle volume fraction increases, the location of the maximum local volume fraction is also affected, moving closer to the wall by adding more particles. More specifically, at $\Phi = 10\%$ the maximum is located at $z = 0.051$, while at $\Phi = 40\%$ the maximum is at $z = 0.034$, approximately half of the particle diameter from the wall. Consequently, the particles that form the dense layer at $\Phi = 40\%$ are in close proximity with the wall. In addition, as the particle volume fraction increases, a second and third maximum appear. Again, this second maximum further from the wall is more pronounced as the value of Φ increases, but its location remains constant at $z = 0.105$ (approximately one and a half particle diameters from the wall). These observations suggest that, as the particle volume fraction increases, the flow conditions lead to the

formation of a second (less dense) particle layer in the vicinity of the wall. The case with Φ = 40% also exhibits two additional smaller maxima, before the profile of the local volume fraction reaches a homogeneous distribution in the bulk of the cavity. In other words, by adding more particles to the flow, more layers are forming before the uniform distribution in the central region of the cavity is reached.

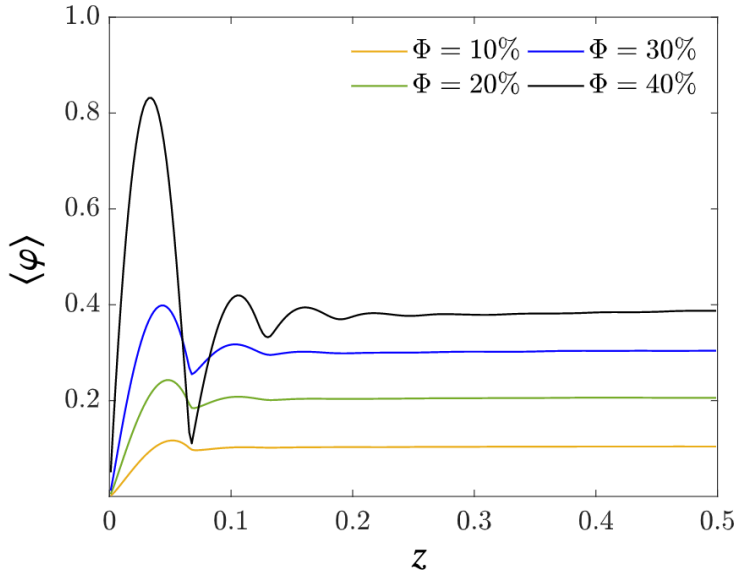

Figure 21. Average local particle volume fraction as a function of the vertical direction for different values of the particle volume fraction specified in this study. In all the cases, d^*_P=1/15.

5. To investigate the effects of particle size, three dimensionless particle diameters are used, d^*_P=1/20, 1/15 and 1/10, for a particle volume fraction of 35%. These values correspond to a free-fall-based Stokes number of (St_f =0.5, 0.9 and 2.1, and a Kolmogorov based Stokes number of (St_K =1.1, 3.5 and 8.1 respectively. The values of both definitions of the Stokes number suggest an increasing influence of the particle inertia relative to the large- and small-scale flow features as the particle size increases. First, the Nusselt number and thermal boundary layer thickness are shown in Figure 22 as a function of the dimensionless particle diameter. As the size of the particle decreases, the Nusselt number decreases significantly and, correspondingly, the thermal boundary layer thickness increases. This weakening of the heat transfer inside the cavity is as dramatic as the Nusselt decrease observed in Figure 20(a) for Φ = 40% and d^*_P=1/15. The main difference observed here is the fact that the rms-based definition of the thermal boundary layer thickness follows the gradient-based definition very closely, in contrast to the findings in Figure 20 where the two definitions deviate. To provide more insight into this pronounced drop in heat transfer, the particle distribution inside the cavity is presented in Figure 23, in the form of averaged local particle volume fraction as a function of the vertical direction z. All three cases share similar characteristics, with a maximum close to the wall and approximately uniform distribution in the bulk of the cavity. As the particle size decreases, the maximum value becomes larger and moves closer to the wall. The maximum values for all the cases occur just above half a particle diameter from the walls. Again, the results for the case with the smallest particles are very similar to what is observed in Figure 21 for Φ = 40% and

d^*_P=1/15. In both these cases, the local particle volume fraction exceeds the value 80% close to the wall. The increased layering next to the walls for smaller particles was also observed in turbulent channel flows [59], albeit not as distinctly as the present study. This finding points to the fact that the strong wall–particle lubrication interaction is more effective with smaller particles, inducing the formation of denser layers next to the walls, influencing the boundary layer region more intensely.

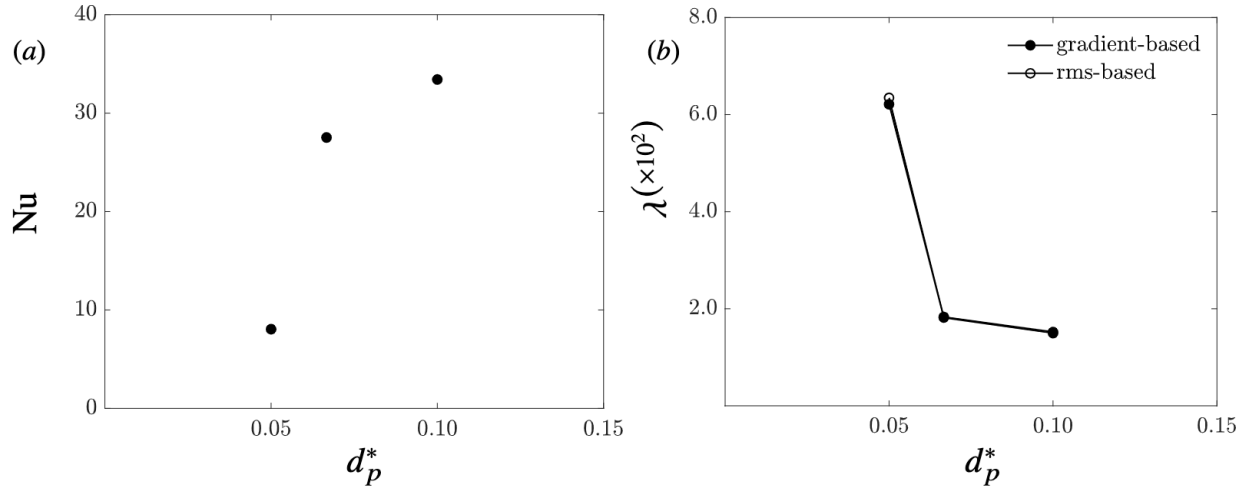

Figure 22. (a) Nusselt number and (b) thermal boundary layer thickness as a function of the dimensionless particle diameter, for Φ = 35%. Both quantities are calculated by averaging the relevant quantities at the bottom and top walls.

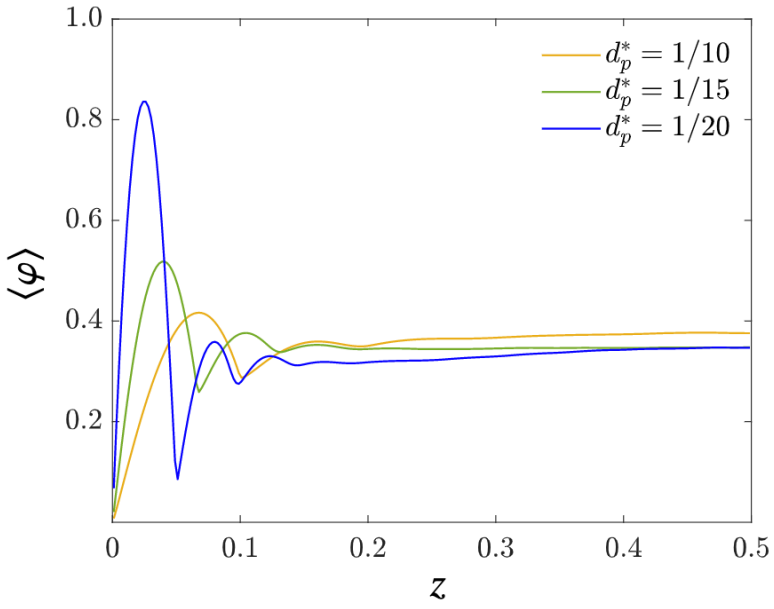

Figure 23. Average local particle volume fraction as a function of the vertical direction for different values of the dimensionless particle diameter. In all the cases, Φ = 35%.

Although the continuum model using nether suspension balance model (SBM) nor DFM could not capture the flow and instabilities in the channel flows. We have also conducted direct numerical simulations (DNSs) and linear stability analysis for neutrally buoyant, non-Brownian and non-colloidal, spherical suspensions concentrated in an incompressible Newtonian viscous fluid. For the very first time, we examined the instability of suspensions flows in both Taylor-Couette flow (TC) and Rayligh-Benard (RB) convection and characterized different regimes of suspension flows. These have been conducted using constitutive laws including both diffusive flux model (DFM) and suspension balance model (SBM). These have been conducted specially to show although the DFM is not capturing the suspensions flows over and through various structures, they can be indeed capturing the particle dynamics and migration in both TC and RB with the existence of particles. The outcomes will impact bioreactor designs and also fuel cells and solar energy systems. These results have already been published in two papers in the *Journal of Fluid Mechanics*, 2021. Recently, we have analyzed different scenarios including the impact of the particle volume fraction and particle size. The outcomes have been accepted to be published in the Royal society transaction A: Special issue related to the Taylor 1923 paper. Some of the outcomes are summarized as follows. All the related manuscripts have been added into the "Production/Articles" section.

3.4. Specific Results on numerical simulations of various suspensions ranging from 10% to 40% in a Taylor-Couette flow using constitutive laws such as suspension balance model (SBM)

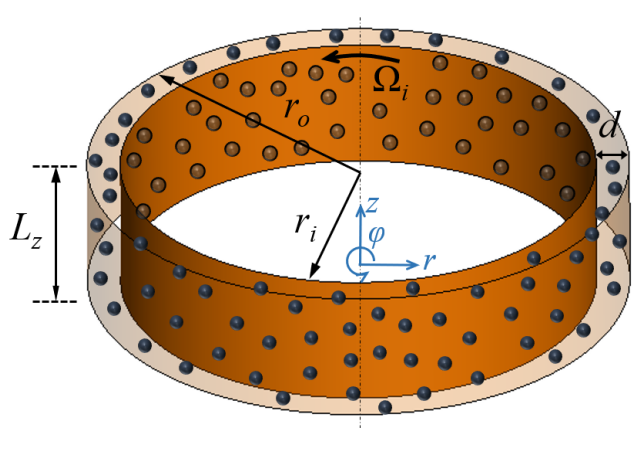

Figure 24. Schematic diagram of a flow of suspensions in Taylor-Couette geometry.

A flow of neutrally buoyant, non-colloidal, rigid, spherical particles concentrated in a viscous fluid of viscosity μ and density ρ has been explored. The suspension of non-colloidal particles is filled in an annulus between two coaxial cylinders of the gap width d with the rotating inner one and the stationary outer one (Figure 24). The radii of the inner and outer cylinders are r_i and r_o(= $r_i + d$), respectively, and the radius ratio ($\eta = r_i/r_o$) is $\eta = 0.877$. The aspect ratio ($\Gamma = L_z/d$) is $\Gamma = 4$ ($\cong 2\lambda_c/d$), where $\lambda_c = 2d$ is the critical wavelength for the flow of a pure Newtonian fluid. We consider concentrated suspensions of $\phi_b = 0.2, 0.3$ with the ratio of annular gap to the particle radius $\epsilon = d/a = 60$, where a is the radius of the suspended particles. As assumed in our previous

study [60, 61], we suppose that the suspensions are in the Stokes flow regime ($Re_p \ll 1$) and in the limit of $Pe \to \infty$, where $Re_p = \rho\dot{\gamma}a^2/\mu$ is the particle Reynolds number based on the fluid shear rate $\dot{\gamma}$ and the radius of the suspended particles a, and $Pe = 6\pi\mu\dot{\gamma}a^3/kT$ is the Péclet number defined with the thermal energy kT.

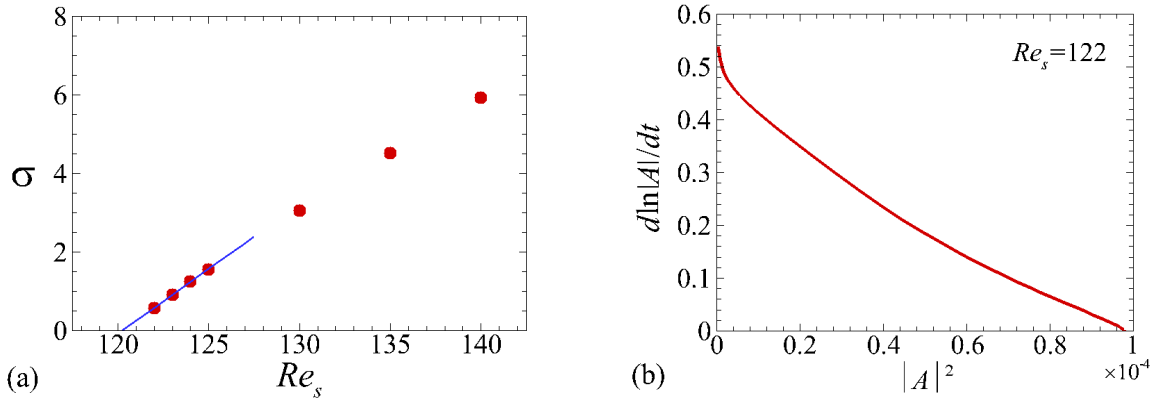

Figure 25. (a) Growth rates of perturbations near the critical Reynolds number for $\epsilon = 60$, (b) The derivative of the amplitude logarithm plotted against the square of the amplitude for $Re_s = 122$, $\epsilon = 60$, and $\phi_b = 0.1$.

1. To characterize the critical states of the flow, we have employed the Landau model which describes the evolution of the flow perturbation in its weakly nonlinear regime and it can be determined as [60, 62-64]

$$\frac{dA}{dt} = \sigma(1 + ic_1)A - l(1 + ic_2)|A|^2A + \cdots, \tag{16}$$

The parameters σ and l represent the linear growth rate of the perturbation and the Landau constant where the sign of l indicates the nature of the bifurcation (i.e., supercritical vs subcritical), and the constant c_1 and c_2 are the linear and nonlinear dispersion coefficients. We introduced the norm of the radial velocity component at the central surface in the annulus to define the amplitude of the perturbation $|A|$, as

$$|A| = \frac{1}{2\pi\Gamma}\int_0^{\Gamma}\int_0^{2\pi} |u_r(r_m, \varphi, z)|\, d\varphi dz, \quad \text{where } r_m = (r_i + r_o)/2 \tag{17}$$

The growth rates (σ) obtained from the evolution of the amplitude $|A|$ for several Re_s near the threshold are plotted in Figure 25(a) where the linear extrapolation gives the critical value of suspension Reynolds number ($Re_{s,c}$). The predicted critical value found to be $Re_{s,c} = 120$ for the suspension of $\epsilon = 60$ and $\phi_b = 0.1$. We also found the same critical Reynolds number for $\epsilon = 200$ which appears the particle size has no influence on the critical Reynolds number. In contrast, [65] found a reduction in critical suspension Reynolds number by increasing the particle size.

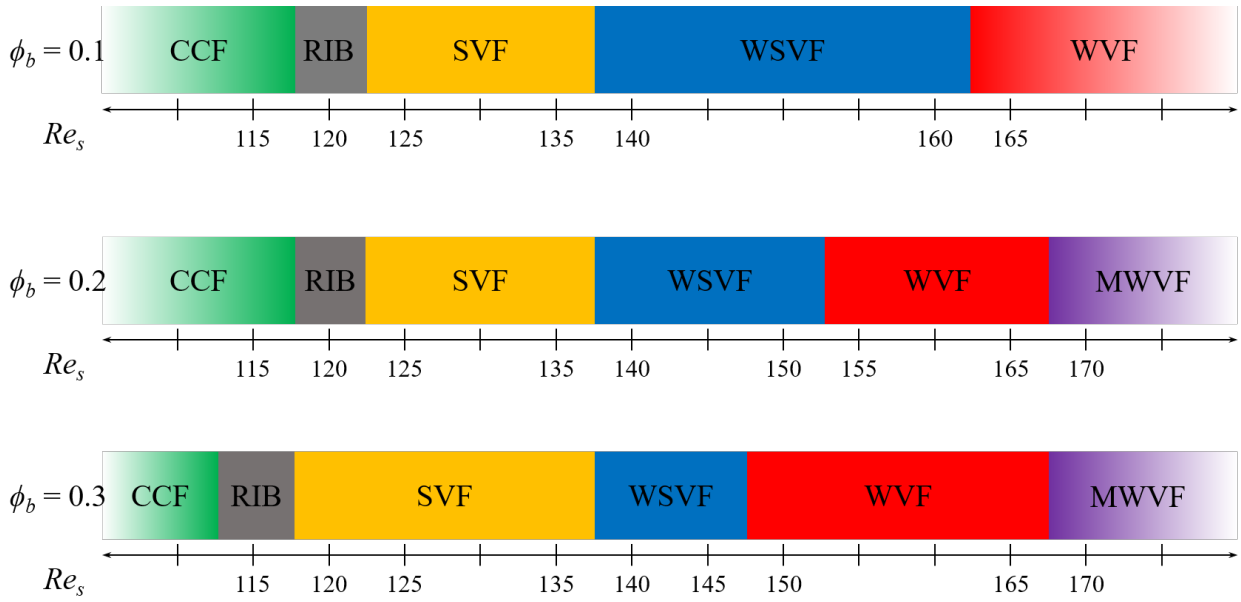

Figure 26. Phase diagrams of flow patterns for suspensions of ϕ_b= 0.1, 0.2 and 0.3 with ϵ = 60.

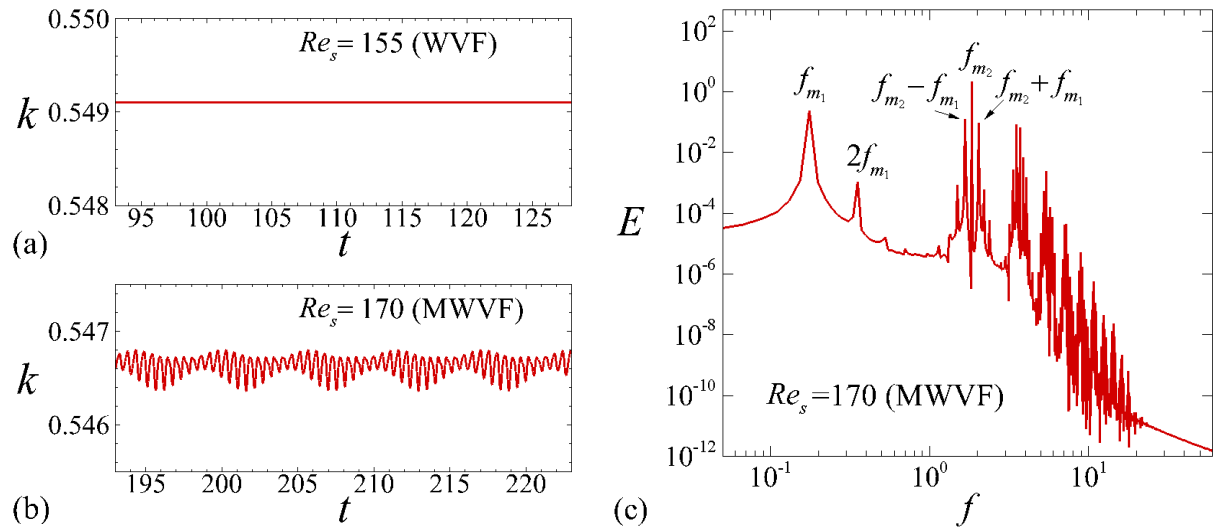

Figure 27. Time variations of the volume-averaged kinetic energy (k) for (a) Re_s= 155 (WVF), (b) Re_s= 170 (MWVF), and (c) the corresponding energy spectrum for Re_s= 170 (MWVF) with ϕ_b= 0.2 and ϵ = 60. Here, we normalized the kinetic energy and the frequency (f) by $(r_i\Omega_i)^2$ and $r_i\Omega_i/d$, respectively.

2. The observed flow patterns are summarized in Fig. 26 with that of the suspension of ϕ_b= 0.1 found in the previous study [60]. As a reminder, a semi-dilute suspension flow of ϕ_b= 0.1 transitions from the CCF via RIB, SVF, and WSVF to WVF, i.e. CCF → RIB → SVF → WSVF → WVF as the Reynolds number (Re_s) increases. Similar to the flow of a semi-dilute suspension, CCF transitions also occur via RIB, SVF, and WSVF to WVF for the flow of concentrated suspensions (ϕ_b= 0.2, 0.3) as shown in Fig. 26. However, another

time-dependent pattern called the modulated wavy-vortex flow appears at higher Reynold numbers ($Re_s \geq 170$).

3. to clearly expose the modulation, variations of the volume-averaged kinetic energy $k = \frac{1}{V}\int u_i u_i \, dV$ with time are displayed in Fig. 27. For the WVF, the kinetic energy is constant in time because the wavy vortices travel to the azimuthal direction constantly (Fig. 27(a)). Note that we found same behaviors in RIB, SVF and WSVF. On the other hand, the kinetic energy oscillates with two different frequencies for the MWVF as given in Fig. 27(b). The frequency can be captured by the corresponding energy spectrum presented in Fig. 27(c). The distinct two dominant frequencies are $f_{m_1} = 0.177$ and $f_{m_2} = 1.853$. The other peaks are combinations of the frequencies. Accordingly, it could be inferred that modulated waves result in the modulated wavy-vortex flow (MWVF).

Bibliography

1. van den Berg, B.M., H. Vink, and J.A. Spaan, *The endothelial glycocalyx protects against myocardial edema.* Circulation research, 2003. **92**(6): p. 592-594.
2. Weinbaum, S., *Models to solve mysteries in biomechanics at the cellular level; a new view of fibre matrix layers.* Ann. Biomed. Eng., 1998. **26**: p. 1-17.
3. Minamiyama, M., *In Vivo Microcirculatory Studies: In Vivo Video Images of Microcirculation Part 2*. 2000.
4. Pries, A.R., et al., *Resistance to blood flow in microvessels in vivo.* Circulation research, 1994. **75**(5): p. 904-915.
5. Pries, A.R., T.W. Secomb, and P. Gaehtgens, *The endothelial surface layer.* Pflügers Archiv, 2000. **440**(5): p. 653-666.
6. Vink, H. and B.R. Duling, *Identification of distinct luminal domains for macromolecules, erythrocytes, and leukocytes within mammalian capillaries.* Circulation research, 1996. **79**(3): p. 581-589.
7. Secomb, T., R. Hsu, and A. Pries, *Motion of red blood cells in a capillary with an endothelial surface layer: effect of flow velocity.* American Journal of Physiology-Heart and Circulatory Physiology, 2001. **281**(2): p. H629-H636.
8. Weinbaum, S., et al., *Mechanotransduction and flow across the endothelial glycocalyx.* Proceedings of the National Academy of Sciences, 2003. **100**(13): p. 7988-7995.
9. Feng, J. and S. Weinbaum, *Lubrication theory in highly compressible porous media: the mechanics of skiing, from red cells to humans.* Journal of Fluid Mechanics, 2000. **422**: p. 281-317.
10. Mirbod, P., Y. Andreopoulos, and S. Weinbaum, *On the generation of lift forces in random soft porous media.* Journal of fluid mechanics, 2009. **619**: p. 147-166.
11. M. Al-Chidiac, P.M.Y.A. and S. Weinbaum, *Dynamic compaction of soft compressible porous materials: experiments on air-solid phase interaction.* Journal of Porous Media, 2009. **12**(11 %! Dynamic compaction of soft compressible porous materials: experiments on air-solid phase interaction %Z Begel House Inc.).

12. Gheisari, R. and P. Mirbod, *Experimental Study of Non-Colloidal Mono and Polydisperse Suspension in Taylor-Couette Flow*. 2014. p. V01DT30A003.
13. Mirbod, P. and D. Meng, *Analysis of bolus formation in micropipette ejection systems.* The European Physical Journal E, 2015. **38**(6): p. 59.
14. Nott, P.R. and B.J. F., *Pressure-driven flow of suspensions: simulation and theory.* Journal of Fluid Mechanics, 1994. **275**: p. 157-199.
15. Morris, J.F. and F. Boulay, *Curvilinear flows of noncolloidal suspensions: The role of normal stresses.* J. Rheology, 1999. **43**: p. 1213.
16. Koh, C.J., H. P., and L. L., *An experimental investigation of concentrated suspension flows in a rectangular channel.* Journal of Fluid Mechanics, 1994. **266**: p. 1-32.
17. Lyon, M.K. and L.G. Leal, *An experimental study of the motion of concentrated suspensions in two-dimensional channel flow. P art 1. M onodisperse systems.* J. Fluid Mech., 1998. **363**: p. 25.
18. Lyon, M.K. and L.G. Leal, *An experimental study of the motion of concentrated suspensions in two-dimensional channel flow. P art 2. B idisperse systems.* J. Fluid Mech., 1998. **363**: p. 57.
19. Leighton, D. and A. A., *The shear-induced migration of particles in concentrated suspensions.* Journal of Fluid Mechanics, 1987. **181**: p. 415-439.
20. Khoshnood, A. and N.A. Jalali, *Long-lived and unstable modes of Brownian suspensions in microchannels.* Journal of fluid mechanics, 2012. **701**: p. 407--418 %! Long-lived and unstable modes of Brownian suspensions in microchannels %Z Cambridge University Press.
21. Goyeau, B., et al., *Momentum transport at a fluid–porous interface.* International Journal of Heat and Mass Transfer, 2003. **46**(21): p. 4071-4081.
22. Hill, A.A. and B. Straughan, *Global stability for thermal convection in a fluid overlying a highly porous material.* Proceedings of the Royal Society A: Mathematical, Physical and Engineering Sciences, 2009. **465**(2101): p. 207-217.
23. Pascal, J., *Linear stability of fluid flow down a porous inclined plane.* Journal of Physics D: Applied Physics, 1999. **32**(4): p. 417.
24. Sadiq, I.M.R. and R. Usha, *Thin Newtonian film flow down a porous inclined plane: Stability analysis.* Physics of Fluids, 2008. **20**(2): p. 022105.
25. Thiele, U., B. Goyeau, and M.G. Velarde, *Stability analysis of thin film flow along a heated porous wall.* Physics of Fluids, 2009. **21**(1): p. 014103.
26. Hill, A.A. and M. Carr, *Nonlinear stability of the one-domain approach to modelling convection in superposed fluid and porous layers.* Proceedings of the Royal Society A: Mathematical, Physical and Engineering Sciences, 2010. **466**(2121): p. 2695-2705.
27. Phillips, R.J., et al., *A constitutive equation for concentrated suspensions that accounts for shear-induced particle migration.* Physics of Fluids A: Fluid Dynamics, 1992. **4**(1): p. 30-40.
28. Segre, G. and A. Silberberg, *Behaviour of macroscopic rigid spheres in Poiseuille flow P art 2. E xperimental results and interpretation.* Journal of fluid mechanics, 1962. **14**(1): p. 136--157 %! Behaviour of macroscopic rigid spheres in Poiseuille flow P art 2. E xperimental results and interpretation %Z Cambridge University Press.
29. Segre, G. and S. A., *Radial particle displacements in poiseuille flow of suspensions.* Nature, 1961. **189**(4760): p. 209.

30. Matas, J.P., J.F. Morris, and Guazzelli, *Inertial migration of rigid spherical particles in P oiseuille flow.* J. Fluid Mech., 2004. **515**: p. 171.
31. Vasseur, P. and R.G. Cox, *The lateral migration of a spherical particle in two-dimensional shear flows.* J. Fluid Mech., 1976. **78**: p. 385 %! The lateral migration of a spherical particle in two-dimensional shear flows %Z Cambridge University Press.
32. Cox, R. and H. Brenner, *The lateral migration of solid particles in Poiseuille flow—I theory.* Chemical Engineering Science, 1968. **23**(2): p. 147-173.
33. Matas, J.P., M.J. F., and G. E., *Lateral force on a rigid sphere in large-inertia laminar pipe flow.* Journal of Fluid Mechanics, 2009. **621**: p. 59-67.
34. Han, M., et al., *Particle migration in tube flow of suspensions.* Journal of rheology, 1999. **43**(5): p. 1157-1174.
35. Hampton, R., et al., *Migration of particles undergoing pressure-driven flow in a circular conduit.* Journal of Rheology, 1997. **41**(3): p. 621-640.
36. Gadala-Maria, F. and A. A., *Shear-induced structure in a concentrated suspension of solid spheres.* Journal of Rheology, 1980. **24**(6): p. 799-814.
37. Mirbod, P., *Two-dimensional computational fluid dynamical investigation of particle migration in rotating eccentric cylinders using suspension balance model.* International Journal of Multiphase Flow, 2016. **80**: p. 79.
38. Kulkarni, P. and M. J., *Suspension properties at finite reynolds number from simulated shear flow.* Phys. Fluids, 2008. **20**(040602).
39. Agelinchaab, M., M. Tachie, and D. Ruth, *Velocity measurement of flow through a model three-dimensional porous medium.* Physics of Fluids, 2006. **18**(1): p. 017105.
40. Arthur, J.K., D.W. Ruth, and M.F. Tachie, *PIV measurements of flow through a model porous medium with varying boundary conditions.* Journal of Fluid Mechanics, 2009. **629**: p. 343-374.
41. Northrup, M.A., K.T. J., and A.S. M., *Fluorescent particle image velocimetry: application to flow measurement in refractive index-matched porous media.* Applied optics, 1991. **30**(21): p. 3034-3040.
42. Gupte, S. and S. Advani, *Flow near the permeable boundary of a porous medium: An experimental investigation using LDA.* Experiments in Fluids, 1997. **22**(5): p. 408-422.
43. Gupte, S.K. and S.G. Advani, *Flow near the permeable boundary of an aligned fiber preform: An experimental investigation using laser Doppler anemometry.* Polymer composites, 1997. **18**(1): p. 114-124.
44. Xi, C. and N.C. Shapley, *Flows of concentrated suspensions through an asymmetric bifurcation.* Journal of Rheology, 2008. **52**(2): p. 625--647 %! Flows of concentrated suspensions through an asymmetric bifurcation %Z The Society of Rheology.
45. Moraczewski, T. and N.C. Shapley, *The effect of inlet conditions on concentrated suspension flows in abrupt expansions.* Physics of Fluids, 2006. **18**(12): p. 123303.
46. Hester-Reilly, H.J. and N.C. Shapley, *Imaging contrast effects in alginate microbeads containing trapped emulsion droplets.* Journal of Magnetic Resonance, 2007. **188**(1): p. 168--175 %! Imaging contrast effects in alginate microbeads containing trapped emulsion droplets %Z Elsevier.
47. Larsen, M.U. and N.C. Shapley, *Stream spreading in multilayer microfluidic flows of suspensions.* Analytical chemistry, 2007. **79**(5): p. 1947--1953 %! Stream spreading in multilayer microfluidic flows of suspensions %Z ACS Publications.

48. Moraczewski, T., H. Tang, and N.C. Shapley, *Flow of a concentrated suspension through an abrupt axisymmetric expansion measured by nuclear magnetic resonance imaging.* Journal of rheology, 2005. **49**(6): p. 1409--1428 %! Flow of a concentrated suspension through an abrupt axisymmetric expansion measured by nuclear magnetic resonance imaging %Z The Society of Rheology.
49. Wiederseiner, S., et al., *Refractive-index and density matching in concentrated particle suspensions: a review.* Experiments in fluids, 2011. **50**(5): p. 1183-1206.
50. Reynolds, O., *III. An experimental investigation of the circumstances which determine whether the motion of water shall be direct or sinuous, and of the law of resistance in parallel channels.* Proceedings of the royal society of London, 1883. **35**(224-226): p. 84-99.
51. Saffman, P., *On the stability of laminar flow of a dusty gas.* Journal of fluid mechanics, 1962. **13**(1): p. 120-128.
52. Haffner, E.A., J. Higham, and P. Mirbod, *Experimental analysis of dilute particle-laden liquids over and through patterned structures.* Bulletin of the American Physical Society, 2019. **64**: p. NP05.00064.
53. Wilkie, T., E. Haffner, and P. Mirbod, *P I V measurements of a dilute suspension flow over and through various porous media models.* Bulletin of the American Physical Society, 2019. **64**: p. M04.00038.
54. Haffner, E.A. and P. Mirbod, *Velocity measurements of dilute particulate suspension over and through a porous medium model.* Physics of fluids, 2020. **32**(8): p. 083608.
55. Reeks, M., *The transport of discrete particles in inhomogeneous turbulence.* Journal of aerosol science, 1983. **14**(6): p. 729-739.
56. Rosti, M.E., P. Mirbod, and L. Brandt, *The impact of porous walls on the rheology of suspensions.* Chemical Engineering Science, 2021. **230**: p. 116178.
57. Zade, S., et al., *Experimental investigation of turbulent suspensions of spherical particles in a square duct.* Journal of Fluid Mechanics, 2018. **857**: p. 748-783.
58. Ardekani, M.N., et al., *Drag reduction in turbulent channel flow laden with finite-size oblate spheroids.* Journal of Fluid Mechanics, 2017. **816**: p. 43-70.
59. Costa, P., et al., *Effects of the finite particle size in turbulent wall-bounded flows of dense suspensions.* Journal of Fluid Mechanics, 2018. **843**: p. 450-478.
60. Kang, C. and P. Mirbod, *Flow instability and transitions in Taylor-Couette flow of a semidilute non-colloidal suspension.* Journal of Fluid Mechanics, 2021. **916**: p. A12.
61. Kang, C. and P. Mirbod, *Non-colloidal suspension Taylor-Couette flows: flow instabilities and hysteresis.* Bulletin of the American Physical Society, 2022.
62. Landau, L.D. and E.M. Lifshitz, *Quantum mechanics: non-relativistic theory*. Vol. 3. 2013: Elsevier.
63. Guckenheimer, J. and P. Holmes, *Nonlinear oscillations, dynamical systems, and bifurcations of vector fields*. Vol. 42. 2013: Springer Science & Business Media.
64. Kang, C., N. Yoshikawa Harunori, and P. Mirbod, *Onset of thermal convection in non-colloidal suspensions.* Journal of Fluid Mechanics, 2021. **915.**
65. Majji, M.V., S. Banerjee, and J.F. Morris, *Inertial flow transitions of a suspension in T aylor-C ouette geometry.* J. Fluid Mech., 2018. **835**: p. 936.